Continuous-time process for human contact dynamics

Robin Persoons,* Matteo D'Alessandro, and Piet Van Mieghem
Faculty of Electrical Engineering, Mathematics and Computer Science, Delft University of Technology, P.O. Box 5031, 2600 GA Delft, The Netherlands

(Received 3 March 2025; accepted 10 July 2025; published 12 September 2025)

Building on the work of Almasan *et al.* [IEEE Trans. Netw. Sci. Eng. **12**, 1649 (2025)], we propose a continuous-time Markov model for human contact dynamics denoted the continuous random walkers induced temporal graph model (CRWIG). In CRWIG, M walkers move randomly and independently of each other on a Markov graph with N nodes in continuous time. If walkers are in the same state (node of the Markov graph) at time t, a link is created between them in their temporal contact graph $G(t)$, where each walker corresponds to one of the M nodes. We define the exact Markov governing equation that describes the movement of the ensemble of M walkers. We investigate the consequences of the time discretization of CRWIG. We prove that CRWIG is characterized by exponential decay of the initial condition and exponentially tailed intermeeting times of the walkers. We investigate two special cases of CRWIG and derive analytical results supported by simulations. We extend the model to allow for nonexponential sojourn times for the single walkers. The non-Markovian model extension of CRWIG is able to reproduce empirical properties of human mobility observed on data: arbitrary flight length distribution, arbitrary pause-time distribution, and intermeeting time distributions that are power-law with an exponential tail.

DOI: 10.1103/lt46-nrh4

I. INTRODUCTION

In the last few decades, the increasing availability of geographical data of human movement has boosted human mobility analysis and studies. Various works focus on the spatial and temporal properties of human mobility patterns [1–5], trying to create models that are able to reproduce empirical mobility patterns or population flows [6]. One driver to understand and model human mobility is the study of epidemic processes. During the COVID-19 pandemic, the quarantining and movement of individuals had a large impact on the spreading process of the virus [7,8]. Yet, nearly all models to compute and predict an epidemic are based on static graphs rather than temporal contact graphs.

Following the ideas in Ref. [9], we propose the continuous random walkers induced temporal graph (CRWIG) model, which employs random walkers on a finite graph to generate temporal contact graphs. In CRWIG, M walkers move randomly and independently of each other on a weighted and directed Markov graph with N nodes in continuous time. Each random walker m in CRWIG executes an instance of a human mobility process, defined by its walker policy, the $N \times N$ infinitesimal generator Q_m. CRWIG then assumes the principle of co-location contacts [8,10]: if walkers are in the same state (node of the Markov graph) at time t, a link is created between them in the temporal contact graph $G(t)$. The contact graph $G(t)$ has M nodes, each corresponding to a walker (see also Fig. 1 in Ref. [9]).

The "Markov graph" on which the M walkers move is a "process graph," not only, e.g., a physical city map. CRWIG is therefore able to abstract the geographical space in which humans move, and each node of the Markov graph can represent any location, event, or activity, whose spatial scale defines a contact. The identification of the proper scales on which humans move [11] and the choice of nodes in the Markov graph are thus very important; otherwise, the co-location assumption is often not correct.

Contrary to Ref. [9], which studies discrete-time RWIG (DRWIG), we focus on the continuous-time Markov process of the ensemble of M walkers. We combine the states of all walkers together and consider the entire M-walker ensemble as a whole, instead of considering the individual walkers separately. The state space of the process is thus N^M dimensional because each walker can potentially be in any of the N states of the Markov graph. The reasons to depart from the discrete time in Ref. [9] are the following: (1) continuous-time models are closer to the "physical" reality and provide the foundations of discrete time models, as discussed in Sec. III; (2) discrete time models become computationally unfeasible if needed at high resolution while the continuous counterpart provides a reliable and efficient framework; (3) many empirical time properties of human mobility, such as pause-times of walkers, intermeeting times of pairs of walkers and the return-time to a hub are defined in continuous-time [1–5] and can easily be encoded in continuous time models (see Sec. V C).

In Sec. II, we define the CRWIG multiwalker mobility process and discuss the structure of the N^M-dimensional state space. In Sec. III, we investigate how the discrete model presented in Ref. [9] is related to the continuous CRWIG model. Section IV extends the results obtained for the discrete DRWIG in Ref. [9] to the continuous-time framework, and we prove new results for CRWIG and DRWIG: the exponential

*Contact author: r.d.l.persoons@tudelft.nl

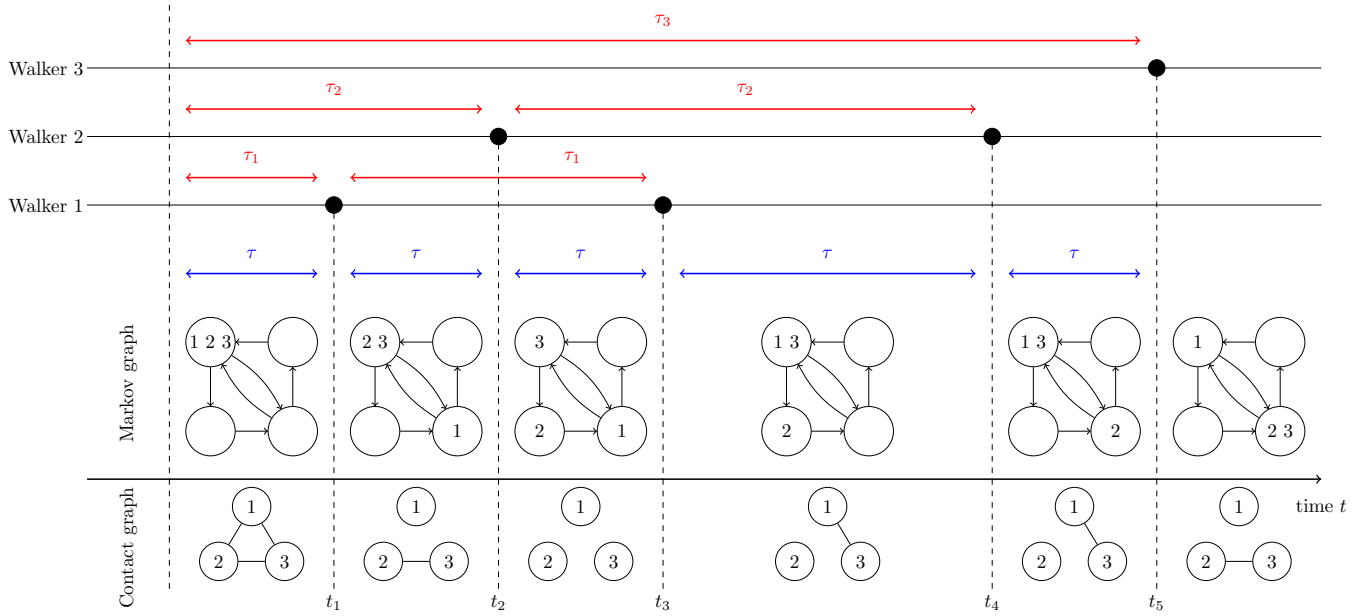

FIG. 1. The transitions of three walkers in the CRWIG model and their sojourn times. The top three horizontal lines are the timelines of the three walkers, where dots indicate the walker changing state. In the middle, the location of the three walkers in the Markov graph is shown, and at the bottom the contact graph that follows after the co-location assumption is depicted. The red arrows indicate the sojourn times τ_m of the individual walkers, while the blue arrows indicate the sojourn times τ of the multiwalker process, which correspond to the times between transitions of any walker.

decay of the influence of the initial state and the exponential tail of the intermeeting time distribution. In Sec. V, we verify some additional analytical results with simulations and show that, after extending CRWIG to allow for arbitrary sojourn time distributions and therefore making it non-Markovian, we can find tail distributions in agreement with observations and measurements of flight lengths, pause times, and intermeeting times. We summarize our findings and discuss our results in Sec. VI.

II. CONTINUOUS-TIME RWIG MARKOV PROCESS

In this section, we define the CRWIG process at the ensemble level. Since the human mobility process is a continuous-time process in CRWIG, any walker can change location (can transition) at any time t. Between transitions, the walkers stay in the same state. This means that the contact graph $G(t)$ remains fixed for some time before changing due to a walker transition and then remains fixed for some time again. In a continuous-time Markov process, the probability of two events happening at the same time is zero, and therefore the process stays in each state for some nonzero amount of time. The (random) time that a continuous-time (Markov) process stays in the same state, before changing to another one, is called a *sojourn time*. In CRWIG three sojourn times have to be distinguished. First, there are the sojourn times τ_m of each walker m, which correspond to the time that walker m stays in the same state. Second, there is the sojourn time τ of the M-walker ensemble, which corresponds to the time between two subsequent transitions of *any* of the m walkers. The multiwalker process, which considers the M-walker ensemble (i.e., the location of all M walkers at the same time), changes state after any walker transition. Lastly, there is the sojourn time τ_G of the contact graph $G(t)$, which corresponds to the time between changes in the contact network. The single- and multiwalker sojourn times are shown in Fig. 1. Figure 1 shows the timelines of three walkers as horizontal lines. The black dots on the lines indicate transitions. The sojourn times of the individual walker mobility processes τ_m are shown in red, while the sojourn times τ of the walker ensemble are shown in blue. In most cases $\tau = \tau_G$, unless a walker moves from a location or state with no other walkers to a different location or state with no other walkers. In Fig. 1 this can be observed at t_4. Only in that case does the contact graph $G(t)$ not change after a walker transition. Because the sojourn times τ_G of the contact graph $G(t)$ are related to the sojourn times τ of the ensemble of walkers and not to those of the individual walkers, we will investigate the multiwalker process of the walker ensemble, rather than the individual single-walker processes.

A. The single- and multiwalker mobility processes

Consider a set $\mathcal{N} = \{1, 2, \ldots, N\}$ of N labeled nodes or states. We define a continuous-time Markovian random walk process generated by Q, a $N \times N$ infinitesimal generator [12], whose elements Q_{ij} represent the rates at which the walker moves from node i to node j, where $j \neq i$. The infinitesimal generator Q assigns to the walker a transition rate from any node i to any other node j in $\mathcal{N}$ and is called the *continuous-time walker policy*. Just as the transition matrix P in a discrete-time mobility process, the infinitesimal generator Q models the human mobility process and describes how the walkers move between states in continuous time.

Let us now consider the process in which M *independent* random walkers move between the nodes in $\mathcal{N}$. The infinitesimal generator Q_m of walker m is equal to minus the Laplacian of a (possibly weighted and directed) graph G_m, whose node set is $\mathcal{N}$ (see, for example, Refs. [12,13]). The single-walker Markov graph G_m describes the topology on which the mth walker moves, determined by its policy Q_m. The single-walker Markov graph G_m has an adjacency matrix A_m whose elements $(A_m)_{ij}$ are equal to the rate Q_{ij} when $i \neq j$ and are zero when $i = j$. If all M walkers have the same policy $Q_m = Q$, CRWIG reduces to a metapopulation model (equivalent to, for example, the definition in Ref. [14], Sec. 5.8). We argue that DRWIG and CRWIG are more general than metapopulation models because, by allowing heterogeneous policies, they no longer describe population flows. We discuss how to restrict the walker policies to an underlying topology in Appendix B.

As illustrated in Fig. 1 with the contact graph sojourn time τ_G, the individual walker processes do not fully characterize the contact graph evolution. We have to consider the multiwalker process, which describes the mobility of all walkers together. Any individual walker m can be in any of the N nodes of its single-walker Markov graph G_m. The state of the M-walker ensemble as a whole can be every possible way in which the M walkers can be distributed over the N states of the node set $\mathcal{N}$. For example, they can all be in states $1, 2, \ldots, N$. Or, $M-1$ walkers can be in state 1 and the mth walker in another state. Each possible distribution of M walkers over the N states in the set $\mathcal{N}$ creates a particular state in the M-walker process. In total, there are N^M such states in the multiwalker mobility process.

Consider the state of the M-walker ensemble, where walker 1 is in state $x_1 \in \mathcal{N}$, walker 2 is in state $x_2 \in \mathcal{N}$, and so on. As in Refs. [15,16], we will write the state of the ensemble as $x_M \ldots x_2 x_1$. If we interpret the state $x_M \ldots x_2 x_1$ as a base-N number, we can enumerate the states of the ensemble from 1 through N^M with the following representation:

$$i = 1 + \sum_{m=1}^{M} (x_m(i) - 1) N^{m-1}, \tag{1}$$

where $x_m(i) \in \{1, \ldots, N\}$ is the single-walker state variable, indicating in which of the N labeled nodes the walker m is found in state i. Compared with the base-N number, we add 1 such that the states are numbered from 1 and subtract $(x_m(i) - 1)$ because the elements of $\mathcal{N}$ are numbered from 1. As an example, consider $M = 4$ walkers on a node set of size $N = 5$:

$$\begin{aligned} x_4 x_3 x_2 x_1 &= 2135, \\ i &= 1 + (4 \times 5^0 + 2 \times 5^1 + 0 \times 5^2 + 1 \times 5^3) \\ &= 140. \end{aligned}$$

In this case, the single-walker state variable $x_1(140) = 5$, $x_2(140) = 3$, $x_3(140) = 1$, and $x_4(140) = 2$, which means that in the ensemble state $i = 140$, walker 1 is in state 5, walker 2 is in state 3, walker 3 is in state 1, and walker 4 is in state 2.

The M-walker process $\{X(t), t \in [0, \infty)\}$, describing the transitions of the M-walker ensemble is itself a Markov process, with an infinitesimal generator $\mathcal{Q}$, which we describe explicitly below. The M-walker process is a combination of all single-walker Markov processes. From each ensemble state i, all single-walker transitions from $x_m(i) = k$ to another state $l \in \mathcal{N}$, which have rate $(Q_m)_{kl}$, correspond to a transition of the multiwalker process out of the multiwalker state i. This transition will go from $i = x_M(i) \ldots x_{m+1}(i)\, k\, x_{m-1}(i) \ldots x_1(i)$ to $j = x_M(i) \ldots x_{m+1}(i)\, l\, x_{m-1}(i) \ldots x_1(i)$ and has rate $(Q_m)_{kl}$. The numbering in (1) allows us to define the elements of the multiwalker infinitesimal generator $\mathcal{Q}$ according to these transitions:

$$\mathcal{Q}_{ij} = \begin{cases} (Q_m)_{pq} & \text{if } i = k + (p-1)N^{m-1},\ j = k + (q-1)N^{m-1}, \\ & k \bmod N^m < N^{m-1},\ p, q = 1, 2, \ldots, N \text{ and } p \neq q \\ \sum_{m=1}^{M} (Q_m)_{x_m(i), x_m(j)} & \text{if } j = i \\ 0 & \text{otherwise.} \end{cases} \tag{2}$$

The infinitesimal generator $\mathcal{Q}$ describes a random walk on the corresponding multiwalker Markov graph $\mathcal{G}$, whose nodes are the N^M states of the multiwalker process. The human mobility process with M walkers, each with its own policy Q_m, is completely equivalent to a single walker moving on the multiwalker Markov graph $\mathcal{G}$. The structure of the ensemble Markov graph $\mathcal{G}$ will depend on the single-walker Markov graphs G_m induced by the single-walker policies Q_m, as illustrated in Fig. 2.

Figure 2 shows a CRWIG process with two walkers. On the left, both single-walker Markov graphs G_1 (shown in red) and G_2 (shown in green) are built with the same $N = 5$ nodes, states, or locations $\{1, 2, 3, 4, 5\} = \mathcal{N}$, here shown as locations on a map of the Netherlands. In the middle, the multiwalker Markov graph $\mathcal{G}$ is shown. The graph $\mathcal{G}$ is a *multilayered graph* consisting of $N = 5$ layers (green circles), each containing the single-walker Markov graph G_1. The *intralayer* links of the multilayered graph correspond to movements of walker 1 (the second number of the state changes while the first stays the same). The *interlayer* links of the multilayered graph correspond to movements of walker 2 (the first number of the state changes while the second stays the same). The detailed view on the right shows the multilayered structure of the multiwalker Markov graph and shows the structure of the interlayer links in particular. To describe the evolution of the M-walker process $X(t)$, we define the single-walker state vectors $s_m(t)$, with elements $(s_m(t))_i = \Pr[X_m(t) = i]$, where $X_m(t)$ is the mth single-walker process and $i \in \mathcal{N}$.

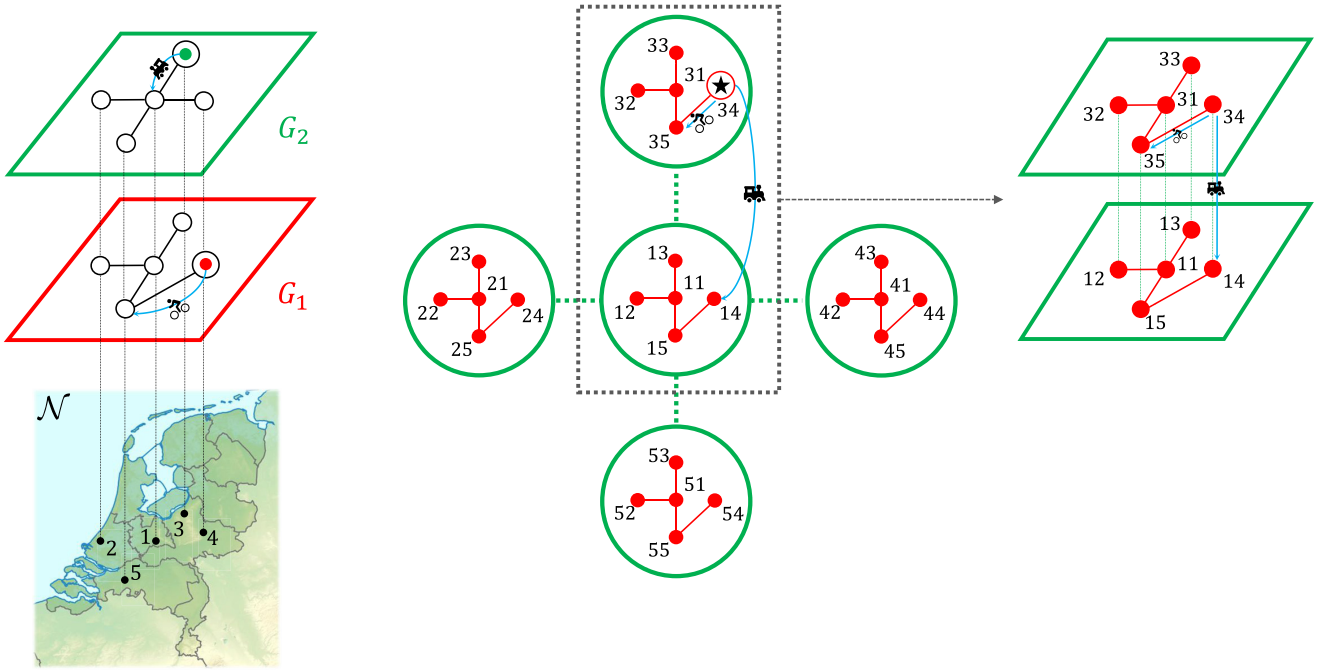

FIG. 2. (left) The Markov graphs G_1 and G_2 of two single-walker processes are shown. The node set $\mathcal{N}$ contains five nodes or states corresponding to five locations on the map [17]. Walker 1 is currently in state 4 (indicated with the red dot in G_1), and walker 2 is currently in state 3 (indicated with the green dot in G_2). Both walkers have only one possible transition from their current state: walker 1 moves from 4 to 5 and walker 2 from 3 to 1. These transitions are indicated with blue arrows with a bicycle and train symbol, respectively. (middle and right) The multiwalker Markov graph is displayed, where each ensemble state i is indicated with $x_2(i)x_1(i)$, which denotes the location of both walkers in that multiwalker state. The multiwalker Markov graph consists of $N = 5$ red copies of G_1, each one corresponding to a node in the node set (map) $\mathcal{N}$. Each copy of G_1 is a layer (green circle) of the multiwalker Markov graph, which is a multilayer graph. Each green circle (layer) corresponds to a position $x_2(i)$ of walker 2, which is the same for all states in the layer. The $N = 5$ layers are connected according to the structure of G_2. The transitions in the multiwalker process corresponding to movements of walker 1 are intralayer links (shown in red), while the transitions corresponding to movements of walker 2 are interlayer links (shown in green). The green link between layers i and j (corresponding to single-walker states i and j) is a simplified visualization of the transitions between the states ik, with $k \in \mathcal{N}$ and jk if $(G_2)_{ij} \neq 0$. The detailed view on the right explicitly shows the interlayer links. The intralayer transitions between nodes belonging to the same layer have the shape of G_1, while the interlayer transitions have the shape of G_2. The state shown on the left (state 34) is indicated with a star in the multiwalker Markov graph, and the transitions shown on the left are also indicated with their respective symbols in both the central figure and the detailed view.

Their evolution is described by the Chapman-Kolmogorov equation [Ref. [12], Eq. (10.19)]:

$$s_m(t) = s_m(0)e^{Q_m t}. \tag{3}$$

Equation (3) describes the probability distribution of the location of walker m at all times t. Similarly, we define the ensemble (or M-walker) state vector $s(t)$, with elements $(s(t))_i = \Pr[X(t) = i]$, where i is one of the N^M ensemble states. The evolution of $s(t)$ is then given by:

$$s(t) = s(0)e^{\mathcal{Q}t}. \tag{4}$$

Due to the independence of the random walkers, we can write

$$\begin{aligned}(s(t))_i = \Pr[X(t) = i] &= \prod_{m=1}^{M} \Pr[X_m(t) = x_m(i)] \\ &= \prod_{m=1}^{M} (s_m(t))_{x_m(i)} = \prod_{m=1}^{M} (s_m(0)e^{Q_m t})_{x_m(i)}.\end{aligned} \tag{5}$$

B. The infinitesimal generator $\mathcal{Q}$ and the adjacency matrix $\mathcal{A}$ of the Markov graph $\mathcal{G}$

In this section, we derive explicit formulas for the multiwalker infinitesimal generator $\mathcal{Q}$ and the adjacency matrix $\mathcal{A}$ of its Markov graph $\mathcal{G}$ as functions of the single-walker policies Q_m and the single-walker Markov graph adjacency matrices A_m, respectively. We add, iteratively, the M walkers to the ensemble one by one, starting with the single-walker process of walker 1. Then, we add the second walker, resulting in the two-walker infinitesimal generator $\mathcal{Q}_2$, which describes the ensemble of walkers 1 and 2. Next, we add the third walker and obtain the three-walker infinitesimal generator $\mathcal{Q}_3$, describing the ensemble of walkers 1, 2, and 3, and so on, until all walkers are added and we arrive at the infinitesimal generator $\mathcal{Q}_M = \mathcal{Q}$ of the M-walker ensemble.

The iterative construction of the multiwalker infinitesimal generator $\mathcal{Q}$ is based on the multilayered structure of its Markov graph $\mathcal{G}$, which is illustrated in Fig. 2 for $M = 2$ walkers. Consider an M-walker CRWIG process. We define the sequence of infinitesimal generators $\{\mathcal{Q}_m\}_{m=1}^{M} = \{\mathcal{Q}_1 = Q_1, \mathcal{Q}_2, \ldots, \mathcal{Q}_m, \ldots, \mathcal{Q}_{M-1}, \mathcal{Q}_M = \mathcal{Q}\}$

as the infinitesimal generators of the CRWIG processes, considering only the first m walkers. These infinitesimal generators $\mathcal{Q}_m$ each have a corresponding Markov graph $\mathcal{G}_m$, which has an adjacency matrix $\mathcal{A}_m$. We emphasize the subtle difference between the symbols for the m-walker infinitesimal generator $\mathcal{Q}_m$ and the single-walker policy Q_m, as well as the subtle difference between the symbols for the m-walker Markov graph adjacency matrix $\mathcal{A}_m$ and the single-walker Markov graph adjacency matrix A_m. The m-walker Markov graphs $\mathcal{G}_m$ have a multilayered structure. Recall that links in a Markov graph correspond to transitions in the process. The structure of the Markov graph $\mathcal{G}_m$ (and in particular $\mathcal{G}_M = \mathcal{G}$) is that of N layers that contain the $(m-1)$-walker Markov graph $\mathcal{G}_{m-1}$. Each layer i corresponds to walker m being in state $i \in \mathcal{N}$. Intralayer links are transitions of the other $m-1$ walkers, all given by $\mathcal{G}_{m-1}$. The interlayer transitions have the shape of the mth-walker single-walker policy G_m, where layers i and j are connected if and only if $(A_m)_{ij} \neq 0$. The connections between layers (interlayer links) have the shape of the identity matrix: the only nodes in $\mathcal{G}_m$ that can be connected between layers are those that correspond to the same node in $\mathcal{G}_{m-1}$ in their respective layers. The structure of the adjacency matrix of the m-walker Markov graph $\mathcal{A}_m$ is

$$\mathcal{A}_m = \begin{bmatrix} \mathcal{A}_{m-1} & I(A_m)_{1,2} & \cdots & I(A_m)_{1,N} \\ I(A_m)_{2,1} & \mathcal{A}_{m-1} & \cdots & I(A_m)_{2,N} \\ \vdots & \vdots & \ddots & \vdots \\ I(A_m)_{N,1} & I(A_m)_{N,2} & \cdots & \mathcal{A}_{m-1} \end{bmatrix}, \tag{6}$$

where I is shorthand for the $N^{m-1} \times N^{m-1}$ identity matrix. The coordinates i and j of each block in the block matrix representation correspond to the single-walker state of walker m. For example, the block $(1, 1)$, which is equal to $\mathcal{A}_{m-1}$, describes the transitions between ensemble-states where walker m is in state 1. This block and all other diagonal blocks describe *intralayer* transitions. Conversely, the block $(1, 2)$, which is equal to $I(A_m)_{1,2}$, describes the transitions from ensemble states where walker m is in state 1, to the ensemble states where walker m is in state 2. This block and all other off-diagonal blocks describe *interlayer* transitions. The element $(A_m)_{i,j}$ connects layers i and j if walker m can transition from a single-walker state i to a single-walker state j, because it is zero otherwise. The identity I links only those ensemble-states from the different layers where no walkers except walker m transition. As an example, we consider again the two-walker system from Fig. 2. The Markov graphs are given by

$$A_1 = \begin{bmatrix} 0 & 1 & 1 & 0 & 1 \\ 1 & 0 & 0 & 0 & 0 \\ 1 & 0 & 0 & 0 & 0 \\ 0 & 0 & 0 & 0 & 1 \\ 1 & 0 & 0 & 1 & 0 \end{bmatrix}, \quad A_2 = \begin{bmatrix} 0 & 1 & 1 & 1 & 1 \\ 1 & 0 & 0 & 0 & 0 \\ 1 & 0 & 0 & 0 & 0 \\ 1 & 0 & 0 & 0 & 0 \\ 1 & 0 & 0 & 0 & 0 \end{bmatrix},$$

$$\mathcal{A} = \begin{bmatrix} A_1 & I_5 & I_5 & I_5 & I_5 \\ I_5 & A_1 & 0 & 0 & 0 \\ I_5 & 0 & A_1 & 0 & 0 \\ I_5 & 0 & 0 & A_1 & 0 \\ I_5 & 0 & 0 & 0 & A_1 \end{bmatrix}.$$

In this example, the structure in (6) can be observed: the identity blocks in $\mathcal{A}$ have the shape of A_2 (interlayer, green in Fig. 2), while the diagonal blocks are A_1 (intralayer, red in Fig. 2). In Appendix C, we give some additional explanation why this construction retains our enumeration (1) at all steps.

We introduce the *Kronecker sum* $\oplus$, which is an operator on a $n \times n$ matrix A and an $m \times m$ matrix B and is defined as $A \oplus B = A \otimes I_m + I_n \otimes B$, where I_k is the $k \times k$ identity matrix and $\otimes$ indicates the Kronecker product (Ref. [18], Sec. B.13). The Kronecker sum allows us to write (6) in a more compact way:

$$\mathcal{A}_m = I_N \otimes \mathcal{A}_{m-1} + A_m \otimes I = A_m \oplus \mathcal{A}_{m-1}, \tag{7}$$

where I_N is the $N \times N$ identity matrix and I represents the $N^{m-1} \times N^{m-1}$ identity matrix. Since the diagonal of A_m is zero for all single-walker Markov graphs, the $A_m \otimes I$ term does not contribute to the diagonal.

Since the structure of the ensemble Markov graph $\mathcal{A}$ and the ensemble infinitesimal generator $\mathcal{Q}$ are similar, we can build $\mathcal{Q}$ iteratively in an analogous way:

$$\mathcal{Q}_m = Q_m \oplus \mathcal{Q}_{m-1} = \begin{bmatrix} \mathcal{Q}_{m-1} + I(Q_m)_{1,1} & I(Q_m)_{1,2} & \cdots & I(Q_m)_{1,N} \\ I(Q_m)_{2,1} & \mathcal{Q}_{m-1} + I(Q_m)_{2,2} & \cdots & I(Q_m)_{2,N} \\ \vdots & \vdots & \ddots & \vdots \\ I(Q_m)_{N,1} & I(Q_m)_{N,2} & \cdots & \mathcal{Q}_{m-1} + I(Q_m)_{N,N} \end{bmatrix}. \tag{8}$$

This means that the closed form of $\mathcal{A}$ and $\mathcal{Q}$ can be written as

$$\mathcal{A} = \bigoplus_{m=M}^{1} A_m, \quad \mathcal{Q} = \bigoplus_{m=M}^{1} Q_m, \tag{9}$$

where the Kronecker sums are in reverse order: $Q_M \oplus Q_{M-1} \oplus \cdots \oplus Q_1$, due to our choice of enumeration in (1).

In Appendix D, we show that the adjacency matrix $\mathcal{A}$ and the infinitesimal generator $\mathcal{Q}$ can be reformulated as rank-$2M$ tensors in the $\mathbb{R}^{\overbrace{N \times N \times \cdots \times N}^{2M \text{ times}}}$ space, which could lead to computational advantages.

III. DISCRETIZATION OF THE CONTINUOUS-TIME RWIG MODEL

We are interested in the differences between CRWIG and the discrete-time RWIG model from Ref. [9] (DRWIG). Because the DRWIG contact graph $G[k]$ is only defined at discrete times $k = 1, 2, \ldots$, the walker policies are transition probability matrices P_m instead of infinitesimal generators Q_m. Each walker m transitions from a state $i \in \mathcal{N}$ at time k to a state $j \in \mathcal{N}$ at time $k+1$ with probability $(P_m)_{ij}$. The DRWIG model explicitly allows multiple walkers to transition in the same timestep from k to $k+1$. This is the first fundamental difference between DRWIG and CRWIG, which

we illustrate with an example. Assume the strongest possible equivalence between the two models: for some time-step Δt we have that at all discrete times $G[k] = G(k\Delta t)$ and all walkers are in the same location, i.e., the processes are in the same ensemble state at every time where the discrete-time model is defined. Consider the following case, where $N = 2, M = 2$ and walker 1 is in location 1, while walker 2 is in location 2 at time 0. Then at time $k = 1$, the walkers have switched places. This means that in DRWIG the contact graphs $G[0] = G[1]$ are equal to the empty graph, implying no contacts happened between the walkers. In CRWIG however, because both walkers transition at the same time with probability zero, one walker must move before the other, guaranteeing that there is at least some nonzero time between $t = 0$ and $t = \Delta t$ that the walkers are in the same location.

We find another fundamental difference between the models by analyzing the discretization of CRWIG.

A. Comparison of discretized processes

We investigate the relation between the CRWIG model in Sec. II A and the DRWIG model in Ref. [9]. Therefore, we will discretize the continuous-time model in multiple ways and investigate the differences. Where continuous-time Markov processes are completely defined by their infinitesimal generator, discrete-time Markov processes are completely defined by their transition probability matrix.

Given an infinitesimal generator Q of a Markov process $\{W(t), t \geqslant 0\}$, the exact transition probability matrix $P(\Delta t)$ of Q over an interval with length Δt follows from the Chapman-Kolmogorov equation [12]

$$P(\Delta t) = e^{Q\Delta t}. \tag{10}$$

This exact transition probability matrix $P(\Delta t)$ describes a discrete-time Markov process $\{W_k(\Delta t), k = 1, 2, \dots\}$ such that $W(k\Delta t) = W_k(\Delta t)$ in distribution if $W(0) = W_0(\Delta t)$. In particular, the M-walker infinitesimal generator $\mathcal{Q}$ is exactly described over discrete steps of size Δt by the multiwalker transition probability matrix $\mathcal{P}(\Delta t)$ given by

$$\mathcal{P}(\Delta t) = e^{\mathcal{Q}\Delta t}, \tag{11}$$

and the single-walker infinitesimal generator Q_m is exactly described over discrete steps of size Δt by the single-walker transition probability matrix $P_m(\Delta t)$ given by

$$P_m(\Delta t) = e^{Q_m\Delta t}. \tag{12}$$

We denote the M-walker continuous-time process defined by $\mathcal{Q}$ as $\{X(t), t \geqslant 0\}$ and the discrete-time Markov process defined by its exact discretization $\mathcal{P}(\Delta t)$ as $\{X_k(\Delta t), k = 1, 2, \dots\}$.

Alternatively to $\mathcal{P}(\Delta t)$, we can define another $N^M \times N^M$ transition probability matrix over steps of size Δt, that we will denote as $\mathbb{P}(\Delta t)$, defined as the combination of the discrete single-walker policies $P_m(\Delta t)$. We denote the discrete-time process defined by $\mathbb{P}(\Delta t)$ as $\{Y_k(\Delta t), k = 1, 2, \dots\}$. In order for $\mathbb{P}(\Delta t)$ to describe the same discrete-time RWIG process as the single-walker policies $P_m(\Delta t)$, it is required that

$$(\mathbb{P}(\Delta t))_{ij} = \prod_{m=1}^{M} (P_m(\Delta t))_{x_m(i),x_m(j)}. \tag{13}$$

Similar to (6) and (8), we can build the m-walker transition probability matrix $\mathbb{P}_m(\Delta t)$ in the $N^m \times N^m$ basis by iteratively adding single walkers at a time. This time, due to the products in (13), the iterative steps are described by the Kronecker product instead of the Kronecker sum:

$$\mathbb{P}_m = P_m \otimes \mathbb{P}_{m-1} = \begin{bmatrix} (P_m)_{1,1}\mathbb{P}_{m-1} & (P_m)_{1,2}\mathbb{P}_{m-1} & \cdots & (P_m)_{1,N}\mathbb{P}_{m-1} \\ (P_m)_{2,1}\mathbb{P}_{m-1} & (P_m)_{2,2}\mathbb{P}_{m-1} & \cdots & (P_m)_{2,N}\mathbb{P}_{m-1} \\ \vdots & \vdots & \ddots & \vdots \\ (P_m)_{N,1}\mathbb{P}_{m-1} & (P_m)_{N,2}\mathbb{P}_{m-1} & \cdots & (P_m)_{N,N}\mathbb{P}_{m-1} \end{bmatrix}, \tag{14}$$

where the dependence on Δt is omitted for clarity. We find

$$\mathbb{P}(\Delta t) = \bigotimes_{m=M}^{1} P_m(\Delta t), \tag{15}$$

where the Kronecker product is indexed in reverse order, consistent with (9) and (14). The equation $\mathbb{P} = \bigotimes_{m=M}^{1} P_m$ is a known expression for the ensemble transition probability of M discrete-time random walkers with policies P_m that can move at the same time (see, for example, Riascos and Sanders [19]).

Instead of the exact discretization, we can define the time-sampled Markov chain [12], with transition probability matrix $\hat{P}(\Delta t) = I + \Delta t Q$, which is the first-order approximation of the Taylor series of $P(\Delta t)$ in (10). We write $\hat{\mathcal{P}}(\Delta t)$ and $\hat{P}_m(\Delta t)$ for the first-order approximations of (11) and (12), respectively, as

$$\hat{\mathcal{P}}(\Delta t) = I + \Delta t \mathcal{Q}, \tag{16}$$

$$\hat{P}_m(\Delta t) = I + \Delta t Q_m. \tag{17}$$

Additionally, we write

$$\hat{\mathbb{P}}(\Delta t) = \bigotimes_{m=M}^{1} \hat{P}_m(\Delta t) \tag{18}$$

and indicate the two discrete-time processes defined by $\hat{\mathcal{P}}(\Delta t)$ and $\hat{\mathbb{P}}(\Delta t)$ as $\hat{X}_k(\Delta t)$ and $\hat{Y}_k(\Delta t)$, respectively.

We prove that the transition matrices (11) and (15) define the same discrete-time process.

Theorem 1. Given M walker policies $Q_1, \dots, Q_M$, the discrete-time process $Y_k(\Delta t)$, described by the transition probability matrix $\mathbb{P}(\Delta t)$, built from the exact single-walker transition probability matrices $P_1(\Delta t), \dots, P_M(\Delta t)$ and the discrete-time process $X_k(\Delta t)$, described by the exact transition probability matrix $\mathcal{P}(\Delta t)$, are the same process. In other words, $X_k(\Delta t) \overset{d}{=} Y_k(\Delta t)$ in distribution, for all $k = 1, 2, \dots$ and for all $\Delta t \geqslant 0$, if $X_0(\Delta t) = Y_0(\Delta t)$.

Proof. We construct both the $N^M \times N^M$ dimensional matrices $\mathcal{P}(\Delta t)$ in (11) and $\mathbb{P}(\Delta t)$ in (15) iteratively and show by induction that they are equal at every step. If both transition probability matrices are the same, then so are the processes $X_k(\Delta t)$ and $Y_k(\Delta t)$.

Considering only the first walker, we have $\mathbb{P}_1(\Delta t) = P_1(\Delta t)$ and $\mathcal{P}(\Delta t) = e^{\mathcal{Q}_1 \Delta t}$, which are the same due to (12). Next, we prove that $\mathbb{P}_m(\Delta t) = \mathcal{P}_m(\Delta t)$ after the induction assumption that $\mathbb{P}_{m-1}(\Delta t) = \mathcal{P}_{m-1}(\Delta t)$. We find that

$$\mathbb{P}_m(\Delta t) = P_m(\Delta t) \otimes \mathbb{P}_{m-1}(\Delta t) = e^{\mathcal{Q}_m \Delta t} \otimes e^{\mathcal{Q}_{m-1} \Delta t}$$

$$= e^{\mathcal{Q}_m \Delta t \oplus \mathcal{Q}_{m-1} \Delta t} = e^{\mathcal{Q}_m \Delta t} = \mathcal{P}_m(\Delta t),$$

where we have used the identity $e^{A \oplus B} = e^A \otimes e^B$ (see, for example, Ref. [18], Theorem 10.9). ■

Conversely, in the time-sampled case, the transition matrices (16) and (18) do *not* define the same discrete-time process.

Theorem 2. Given M walker policies $Q_1, \ldots, Q_M$, the discrete-time process $\hat{Y}_k(\Delta t)$ described by the transition probability matrix $\hat{\mathbb{P}}(\Delta t)$, built from the time-sampled single-walker transition probability matrices $\hat{P}_1(\Delta t), \ldots, \hat{P}_M(\Delta t)$ and the discrete-time process $\hat{X}_k(\Delta t)$, described by the time-sampled transition probability matrix $\hat{\mathcal{P}}(\Delta t)$, are *not* the same process if at least two walkers have a nondiagonal (nonstationary) policy.

Proof. We denote two walkers with nondiagonal policies as walkers k and l. Assume walker k has a nonzero transition rate $(Q_k)_{ab}, a \neq b$ and walker l has a nonzero transition rate $(Q_l)_{cd}, c \neq d$. Consider a transition from a state i with $x_k(i) = a$ and $x_l(i) = c$ to a state j where $x_k(j) = b$ and $x_l(j) = d$. Then, there are two transitions required to move from state i to state j and thus $\mathcal{Q}_{ij} = 0$ [see (2)]. The time-sampled transition probability matrix $\hat{\mathcal{P}}(\Delta t)$ has the exact same structure as $\mathcal{Q}$ and therefore $(\hat{\mathcal{P}}(\Delta t))_{ij} = 0 \Leftrightarrow \mathcal{Q}_{ij} = 0$.

The time-sampled transition probability matrices $\hat{P}_1(\Delta t), \ldots, \hat{P}_M(\Delta t)$ similarly have the same structure as the policies $Q_1, \ldots, Q_M$. Therefore, we know that $(\hat{P}_k(\Delta t))_{ab} > 0$ and $(\hat{P}_l(\Delta t))_{cd} > 0$. Since the rows of every walker policy $\hat{P}_m(\Delta t)$ sum to one, we can find, for each walker $m \neq k, l$, a transition $(\hat{P}_m(\Delta t))_{y(m),z(m)} > 0$. Consider the state r, defined such that $x_m(r) = y(m)$ for all $m \neq k, l$ and $x_k(r) = a, x_l(r) = c$. In addition, consider the state q, defined such that $x_m(q) = z(m)$ for all $m \neq k, l$ and $x_k(q) = b, x_l(q) = d$. Then, by construction, $(\hat{P}_m(\Delta t))_{x_m(r),x_m(q)} > 0$ for all m and therefore $(\hat{\mathbb{P}}(\Delta t))_{rq} = \prod_{m=1}^{M} (\hat{P}_m(\Delta t))_{x_m(r),x_m(q)} > 0$, where we have used (13).

However, $(\hat{\mathcal{P}}(\Delta t))_{rq} = 0 \neq (\hat{\mathbb{P}}(\Delta t))_{rq}$, because r and q satisfy the definition of i and j above by construction. The processes $\hat{Y}_k(\Delta t)$ and $\hat{X}_k(\Delta t)$ are only the same if they are described by the same transition probability matrix and, therefore, the processes are different. ■

Riascos and Sanders [19] consider an alternative to (15) in which the m walkers cannot move at the same time. Instead, one walker is picked uniformly at random to move the next step. The *asynchronous* walkers have an ensemble transition probability matrix given by

$$P = \frac{1}{M} \sum_{m=1}^{M} \underbrace{I \otimes \cdots \otimes \overbrace{P_m}^{m\text{th position}} \otimes \cdots \otimes I}_{M \text{ terms}},$$

which is similar in definition to our tensor representation in Appendix D, but with the Kronecker product instead of the tensor outer product. We choose not to further investigate the *asynchronous* multiwalker process, because the uniform walker selection does not agree with the continuous-time process, where the walker selection is based on the transition rates. It is also unrelated to the DRWIG model, which explicitly allows synchronous walker transitions.

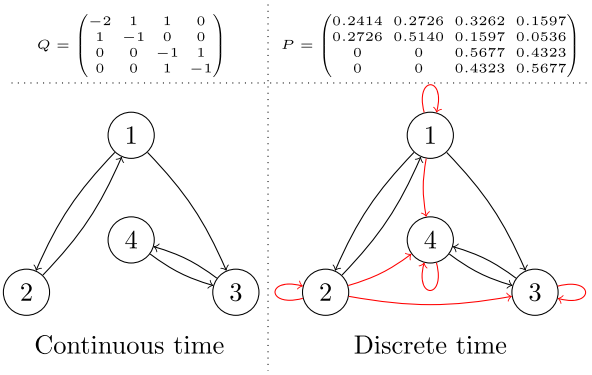

FIG. 3. Single-walker infinitesimal generator Q and its exact transition probability matrix P for $\Delta t = 1$. All transitions in the discrete Markov graph that are not part of the Markov graph in the continuous process are colored red.

B. Loss of topology after discretization

An important consequence of the discretization of the continuous-time process is that the transition probability matrices from (11) and (12) contain transitions that are only possible by multiple transitions in $\mathcal{Q}$ and/or $Q_1, \ldots, Q_M$. This means that the single-walker Markov graphs $G_1, \ldots, G_M$ are *not* the Markov graphs corresponding to the transition matrices $P_1, \ldots, P_M$. This is the second fundamental difference between CRWIG and DRWIG: the discrete-time process that has the same distribution $X(k\Delta t) = X_k(\Delta t)$ as the continuous-time process defined by $\mathcal{Q}$ must allow multiple-hop transitions. When the transition probability matrices $P_1, \ldots, P_M$ are interpreted as in Ref. [9], namely as single-hop transitions, the discrete-time walkers are *walking on a different graph* compared to the walkers on the original continuous-time process, as exemplified in Fig. 3. In Fig. 3, the single-walker infinitesimal generator Q and its topology are shown on the left, while on the right, the exact transition probability matrix $P(1) = e^Q$ is shown for $\Delta t = 1$, together with its topology. In red, the links that are not present in the topology of Q are shown. The self-loops are imposed by the discrete-time process, but the other links can be interpreted as single-hop paths and thus as part of the network the walker walks on, even though the "ground truth" continuous-time topology is different. For large enough Δt, the weight of the links between nodes 1 and 2 and the self-loops in nodes 1 and 2 will tend to zero, effectively removing them from the

network, and, hence, deviating even more compared to the "ground truth".

C. CRWIG and DRWIG

Our results on the discretization of CRWIG may raise questions about its relevancy. One may ask why we need CRWIG if an exact discretization exists. This question is important to address.

We argue that CRWIG is relevant from a modeling point of view. The physical reality of human mobility occurs in continuous time, like any physical process. Therefore, a discrete-time model is an approximation. The approximation is only accurate if the time step Δt is (very) small. Firstly, with small Δt time steps, simulating a continuous-time process is significantly easier than simulating the corresponding discrete-time process. In the continuous-time process, the sojourn time of each walker is generated immediately after they move. For each single-walker transition two random variables have to be sampled: the sojourn time τ_m (or time before next movement) and the destination of the next transition. In the discrete-time process a random variable has to be sampled for each walker after each step Δt, namely the location of each walker after the next time step Δt. Approximately $E[\tau_m]/2\Delta t$ times more samples must be drawn from a probability distribution in the discrete-time process. Secondly, a discrete-time model with small time steps Δt is hard to construct, unless the equivalent continuous-time model is known. The difficulty stems from the fact that, at small Δt, the policies P_m are almost identical to the identity matrix, which makes them very hard to interpret and, indeed, create.

If human mobility is described by our Markovian continuous-time CRWIG model, then the search space when training a discrete-time version on discrete data [20] can be strongly reduced. All walker policies assume the form $P_m = e^{Q_m \Delta t} = \sum_{k=0}^{\infty} \frac{(Q_m)^k}{k!}(\Delta t)^k$ for some set of infinitesimal generators Q_m and a single time step Δt, where the kth power of Q_m corresponds to the rate of k-hop paths. It follows from $P_m = e^{Q_m \Delta t}$ that (1) if $(P_m)_{ij} > 0$ and $(P_m)_{jk} > 0$, then $(P_m)_{ik}$ must be larger than zero as well (proved in Appendix A 1); (2) since Δt is finite, $(P_m)_{ii}$ must be larger than zero, and when $(P_m)_{ii} > 0$, then $(P_m)_{ij} < 1$ except if $i = j$ and i is an absorbing state. If P_m is a discretization of a CRWIG policy Q_m, then the continuous-time model can be used to interpolate the discrete-time process if one wants to reduce the step size Δt. This can be required for accurate modeling of dynamic processes on the CRWIG contact network. For example, in a respiratory epidemic Δt should be in the order of minutes [21–23] to correctly take into account all the relevant contacts. We emphasize that interpolation is generally not possible in the discrete-time framework, because it would require solving $P_m(\Delta t) = P_m(\frac{\Delta t}{K})^K$, which is equivalent to taking the Kth root of the transition probability matrix $\sqrt[K]{P_m(\Delta t)}$, which does not necessarily exist and may not be unique.

IV. ANALYTICAL RESULTS

In this section, we show some analytical results related to the contact graph distribution and intermeeting times in CRWIG. First, we show continuous-time analogues to the two main theorems in Ref. [9] that describe the distribution of the contact graph $G(t)$ at a given time t. Second, we show that the dependence of the distribution of the contact graph $G(t)$ on the initial condition decays exponentially fast. Thirdly, we consider the intermeeting times of two walkers and show that the intermeeting times are not heavy-tailed.

A. Brief review of DRWIG results

Most DRWIG results from Almasan *et al.* [9] hold in continuous time, although some minor adjustments are needed in some cases. The results about co-location transfer directly, such as the number of possible contact graphs as a function of N and M. Other results can be translated to continuous time, because they are based on the single-walker state vector $s_m[k]$. By replacing the discrete-time single-walker state vector $s_m[k] = s_m[0]P_m^k$ with the continuous-time single-walker state vector $s_m(t) = s_m(0)e^{Q_m t}$, analogous continuous-time results of the main results in Ref. [9] follow directly. In particular, Theorem 1 and the main result, Theorem 2, from [9] have continuous-time equivalents, which we state below. We first define the probability that a set of walkers is in the same single-walker state.

Definition 3. Consider a set (or clique) of walkers C. The probability that the walkers of the set C are in the same location at time t, denoted as $\sigma_C(t) = \sum_{i\in\Omega_C}[s(0)e^{\mathcal{Q}t}]_i$, where Ω_C is the set of the M-walker states where the walkers in the set C share a location.

The same definitions of clique-sets $\{C_1, C_2, \ldots, C_k\}$ and partitions as in Ref. [9] are transferred to the continuous versions of the two main theorems.

Theorem 4 (Continuous version of Theorem 1 in [9]). The probability of a k-clique contact graph $G = \{C_1, C_2, \ldots, C_k\}$ at time t is

$$\Pr[G(t) = G] = \sum_{i_1=1}^{N} \sum_{\substack{i_2=1 \\ i_2\notin\{i_1\}}}^{N} \cdots \sum_{\substack{i_k=1 \\ i_k\notin\{i_l\}_{l=1}^{m-1}}}^{N} \prod_{j=1}^{k} \prod_{m\in C_j} (s_m(t))_{i_j}. \quad (19)$$

Theorem 5 (Continuous version of Theorem 2 in [9]). The probability of a k-clique contact graph $G = \{C_1, C_2, \ldots, C_k\}$ at time t is

$$\Pr[G(t) = G] = \sum_{\pi\in P_G} \left(\prod_{\mathcal{C}\in\pi} (-1)^{|\mathcal{C}|-1}(|\mathcal{C}|-1)! \right) \prod_{C\in G(\pi)} \sigma_C(t), \quad (20)$$

where $|\mathcal{C}|$ denotes the number of cliques C of partition π on $G = \{C_1, C_2, \ldots, C_k\}$.

We used (19) to verify our simulations of CRWIG. In Fig. 4 the distribution of the contact graph $G(t)$ over time is shown for $M = 3$ walkers with randomized policies Q_m with $N = 6$ locations. Each policy Q_m is minus the weighted Laplacian of an Erdős-Rényi graph of size $N = 6$ with link probability $p = 1/2$ and random directed link weights uniform in $[0, 1]$.

B. Decay of the initial condition

The probability that the contact graph $G(t)$ equals G, conditioned on the initial condition $G(0) = G^*$, written as $\Pr[G(t) = G|G(0) = G^*]$, decays exponentially to the steady-

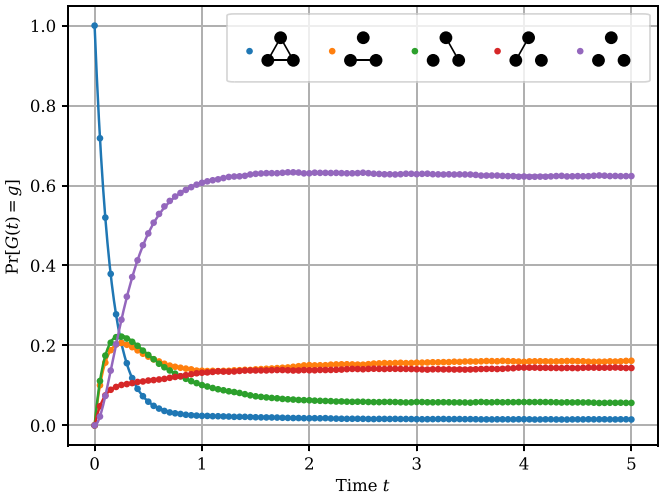

FIG. 4. Distribution of all possible graphs of size $M = 3$ generated by CRWIG over time. Each walker has a policy generated by adding random rates uniform from the interval [0, 1] to the directed links of an Erdős-Rényi graph of size $N = 6$ with link probability $p = 1/2$. The lines show the theoretical distribution from (19), while the dots show simulation results averaged over 10^5 simulations. Each color corresponds to one of the five possible contact graphs on $M = 3$ nodes. At $t = 0$ all walkers are in the same location.

state probability $\Pr[G(\infty) = G]$ as $t \to \infty$ if the steady state is unique. A unique steady state is required because otherwise the steady state distribution $\lim_{t\to\infty} \Pr[X(t) = i] = (s_\infty)_i = \pi_i$ is not well-defined. In continuous-time, a unique steady state is equivalent to requiring that the Markov graph has a single strongly connected component that can be reached from all nodes. The exponential decay also occurs in DRWIG, in which case the assumption of a unique steady state requires that the transition matrix $\mathbb{P}$ is aperiodic and irreducible. We treat both cases in this section under the assumption that $\mathbb{P}$ and $\mathcal{Q}$ are diagonalizable. The arguments for the diagonalizable case are very similar to the general case, which requires the introduction of Jordan forms. Since the diagonalizable case presents the arguments well enough, the general case is treated in Appendix A 2.

We define the set of states in the M-walker process that correspond to the contact graph G as Ω_G [i.e., those states i such that $X(t) = i$ implies that $G(t) = G$]. Assume that the state of the M-walker process at time $t = 0$ is $g \in \Omega_{G^*}$, then

$$\Pr[G(t) = G|X(0) = g] = \Pr[X(t) \in \Omega_G|X(0) = g] = \sum_{\omega\in\Omega_G} (e^{\mathcal{Q}t})_{g\omega}.$$

After diagonalization of $e^{\mathcal{Q}t}$, the last term can be rewritten [Ref. [12], Eq. (10.16)] as

$$\Pr[G(t) = G|X(0) = g] = \sum_{\omega\in\Omega_G} \pi_\omega + \sum_{k=2}^{N^M} e^{\lambda_k t}\left(x_k y_k^T\right)_{g\omega},$$

where π is the steady-state vector of the M-walker ensemble. Each term in the second sum will decay to zero exponentially because the eigenvalues λ_k of the infinitesimal generator $\mathcal{Q}$ have a negative real part [12]. The same result can be shown to hold for DRWIG if the transition probability matrix $\mathbb{P}$ is aperiodic and irreducible. Then, it follows [12] that the eigenvalues of $\mathbb{P}$ are $\lambda_1 = 1 > |\lambda_2| \geqslant |\lambda_3| \geqslant \cdots \geqslant |\lambda_{N^M}|$. Assuming that $\mathbb{P}$ is diagonalizable, we find [12]

$$\mathbb{P}^k = u\pi + \sum_{l=2}^{N^M} \lambda_l^k x_l y_l^T$$

and thus

$$\Pr[G[k] = G|X[0] = g] = \sum_{\omega\in\Omega_G} (\mathbb{P}^k)_{g\omega} = \sum_{\omega\in\Omega_G} \pi_\omega + \sum_{l=2}^{N^M} \lambda_l^k \left(x_l y_l^T\right)_{g\omega},$$

where each term in the second sum will decay to zero exponentially since $|\lambda_l| < 1$ for all $l > 1$.

C. Intermeeting times

A commonly used metric in mobility processes is the *intermeeting time*, which is the (random) time between two contacts of a pair of individuals. Data shows [3,4] that human contacts often have a power-law intermeeting time distribution with an exponential tail. We show that CRWIG always has exponentially tailed intermeeting times.

Assume that both walkers m and n are in the single-walker state i and walker n moves to state j different from state i. We will call the time of this transition $t = \eta$ and define the intermeeting time $T_{m,n}$ as

$$T_{m,n} = \inf\{t - \eta : X_m(t) = X_n(t)|X_m(\eta) = i, X_n(\eta) = j \neq i, X_n(\eta - \epsilon) = i \quad \text{for } \epsilon \downarrow 0\}. \quad (21)$$

Since the walkers m and n are independent of all other walkers, we can define the intermeeting time $T_{m,n}$ in terms of the two-walker process. The subset Ω_{mn} of the N^2-dimensional state space, where walkers m and n are in the same single-walker state, is defined as

$$\Omega_{mn} = \{i : x_m(i) = x_n(i)\}. \quad (22)$$

We write Ω_{mn}^C for the complement of Ω_{mn}:

$$\Omega_{mn}^C = \{i : x_m(i) \neq x_n(i)\}. \quad (23)$$

We apply (22) and (23) to rewrite (21) in terms of the two-walker continuous time process $X(t)$:

$$T_{m,n} = \inf\{t - \eta : X(t) \in \Omega_{mn}|X(\eta) \in \Omega_{mn}^C, X(\eta - \epsilon) \in \Omega_{mn} \quad \text{for } \epsilon \downarrow 0\}. \quad (24)$$

To prove the intermeeting times are not heavy-tailed, we shift our view from realizations of the CRWIG process to walks on its Markov graph and introduce a few definitions. Consider the two-walker CRWIG process with infinitesimal generator $\mathcal{Q}_2$. We define the (random) intermeeting walk $W(m, n)$, which is a walk through the Markov graph of the two-walker process, with length $|W(m, n)| = l(W)$ as a sequence of states $\{w_1, w_2, \ldots, w_{l(W)}\}$ such that $w_i \neq w_{i+1}$ for all $i = 1, \ldots, l(W)$ and $w_1, w_{l(W)} \in \Omega_{mn}$, $w_i \in \Omega_{mn}^C$ for all $i \neq 1, l(W)$. The intermeeting walks are subsequences of the sequence of states of the CRIWG process during a realization,

specifically those who start in Ω_{mn} and end the first time Ω_{mn} is reached afterwards. Indeed, each time walkers m and n meet again in a realization of CRWIG there is an intermeeting time $T_{m,n}$ (the time between the two meetings) and an intermeeting walk W (the sequence of states through which the process went between meetings). We prove the following lemma:

Lemma 6. The distribution of the intermeeting walk length $\Pr[l(W) = k]$ of two arbitrary walkers in the CRWIG process is bounded by an exponential:

$$\Pr[l(W) = k] \leqslant Ce^{-ak}, \tag{25}$$

where a and C are real, finite constants larger than zero.

Proof. See Appendix A3. ■

The proof in Appendix A3 also applies to prove that DR-WIG intermeeting times (which are equivalent to intermeeting walk lengths in discrete time) are not heavy-tailed by considering the two-walker discrete-time Markov graph, instead of the continuous-time one. Using Lemma 6, we can prove that CRWIG intermeeting times are also exponentially tailed.

Theorem 7 (The CRWIG intermeeting times are not heavy-tailed). Consider an M-walker CRWIG process with infinitesimal generator $\mathcal{Q}$ and single-walker policies $Q_1, Q_2, \ldots, Q_M$. Consider two walkers m and n. We denote with $\mathcal{Q}_2(m,n)$ the two-walker infinitesimal generator of walkers m and n and write Θ for the smallest nonzero and nondiagonal element of $\mathcal{Q}_2(m,n)$. Then, the tail probability $\Pr[T_{m,n} > x] = 1 - F_{T_{m,n}}(x)$ of the intermeeting time $T_{m,n}$ is bounded as

$$\begin{aligned}\Pr[T_{m,n} > x] = 1 - F_{T_{m,n}}(x) &\leqslant \sum_{k=1}^{\infty} Ce^{-ak} \sum_{r=0}^{k-1} \frac{1}{r!} e^{-\Theta x} (\Theta x)^r \\ &\leqslant \tilde{C} e^{-(1-\xi)\Theta x},\end{aligned} \tag{26}$$

where $F_{T_{m,n}}(x)$ is the distribution of $T_{m,n}$, ξ is a constant between 0 and 1 and $\tilde{C} < \infty$.

Proof. See Appendix A4. ■

While the sojourn times of the Markovian CRWIG are exponential, other M-walker processes with the same structure (i.e., no transitions occur that can't occur in CRWIG) could have heavy-tailed sojourn times. We show that heavy-tailed sojourn times imply heavy-tailed intermeeting times. Below, the notation $f(x) \sim g(x)$ means $\lim_{x\to\infty} \frac{f(x)}{g(x)} = 1$.

Theorem 8. Consider an M-walker process with heavy-tailed sojourn time distributions, i.e., $\Pr[\tau_i > x] \sim c_i x^{-\alpha_i}$, where τ_i is the sojourn time of the M-walker ensemble state i and $\alpha_i, c_i \in (0, \infty)$ are constants. Consider two walkers m and n. Then, the intermeeting times $T_{m,n}$ are heavy-tailed.

Proof. We show that $\Pr[T_{m,n} > x] \geqslant \Pr[\tau_{j(x)} > x] \sim c_\zeta x^{-\alpha_\zeta}$ for some state ζ, where $j(x) := \operatorname{argmin}_j \Pr[\tau_j > x]$ (if multiple j minimize the expression $j(x)$ is defined as the smallest of them). We observe that $\Pr[T_{m,n} > x]$ is larger or equal to the sojourn time of the first state between the meetings. We denote with ξ the first state where walkers m and n are in different locations [$X(\eta)$ in equation (24)]. Then,

$$\Pr[T_{m,n} > x] \geqslant \Pr[\tau_\xi > x] \geqslant \Pr[\tau_{j(x)} > x].$$

The variable $j(x)$ converges for $x \to \infty$ because $\lim_{x\to\infty} \frac{c_i x^{-\alpha_i}}{c_j x^{-\alpha_j}}$ is well defined for all states i, j and orders the probabilities $\Pr[\tau_j > x]$ for (very) large x. Specifically $j(x)$ converges to ζ, where ζ has $\alpha_\zeta = \max_i \alpha_i$ and $c_\zeta \leqslant c_k$ for all k which have $\alpha_k = \alpha_\zeta$. This gives the tail $\Pr[\tau_{j(x)} > x] \sim c_\zeta x^{-\alpha_\zeta}$. ■

We emphasize that, if the walkers are independent, the sojourn times τ_i of the M-walker ensemble can only be heavy-tailed if the sojourn times of all individual walkers are heavy-tailed. Otherwise, the tail of the M-walker sojourn times would be destroyed by the non-heavy-tailed transition(s).

V. SIMULATIONS

A. Symmetric versus nonsymmetric walker policies

In this section, we discuss symmetric walker policies Q_m, which correspond to undirected Markov graphs G_m. Caution is required when using symmetric policies, because every walker with a symmetric policy has the same steady-state distribution $\pi_m = \frac{1}{N}u$, where u is the all-one vector. Using an undirected and unweighted graph as the Markov graph G_m yields a symmetric policy Q_m. This implies that common undirected graph models such as ER-graphs, BA-graphs, WS-graphs, stochastic block models, etc. should be used with caution to generate the single-walker Markov graphs G_m. First, we discuss the physical downsides of undirected or symmetrical graphs. Second, we suggest a simple method to modify undirected graphs to directed graphs, which works better if a graph is less regular. Lastly, we illustrate our findings with an experiment.

It is a known result that the steady-state vector of a symmetric infinitesimal generator Q is the all-1 vector u.

Theorem 9. The steady-state vector π_m of walker m, with symmetric policy Q_m, such that $(Q_m)^T = Q_m$, is given by $\pi_m = \frac{1}{N}u$, where u is the all-1 vector.

Proof. Since Q_m is an infinitesimal generator, the left eigenvector y_1 of eigenvalue $\lambda_1 = 0$ is the steady-state vector $(\pi_m)^T$. The right eigenvector x_1 of eigenvalue $\lambda_1 = 0$ is u, the all-1 vector. Because Q_m is symmetric, the left and right eigenvectors are the same, and thus $\pi_m = \frac{1}{N}u$, where the constant $\frac{1}{N}$ follows from the requirement that $\sum_{i=1}^{N}(\pi_m)_i = 1$. ■

The steady-state of the ensemble is also uniform if all M walkers have a symmetric policy, because $\mathcal{Q}$ is then also symmetric. Alternatively, it follows from (5) that the ensemble steady-state probability of state i is given by

$$\pi_i = (s_\infty)_i = \prod_{m=1}^{M} ((s_m)_\infty)_{x_m(i)} = \prod_{m=1}^{M} \frac{1}{N} = \frac{1}{N^M}.$$

We emphasize that (a) the steady-state vector $s_\infty = \frac{1}{N^M}u$ does not imply that the steady-state contact graph distribution $\Pr[G_\infty = G]$ is also uniform. Instead, the probability of a contact graph G with C cliques is $\frac{N!}{(N-C)!N^M}$, which is $1/N^M$ times the number of arrangements of the M walkers across the N locations that create the graph [9]. (b) The result holds for any set of symmetric policies Q_m, even if walkers have different policies.

A uniform steady state is generally not realistic because it implies that the walker spends the same amount of time in each location on average. However, we emphasize that the steady-state distribution only describes *average* behavior.

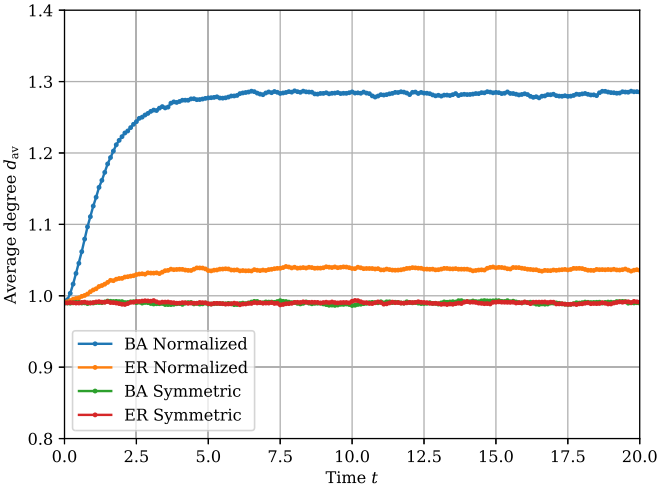

FIG. 5. The average contact graph degree d_{av} over time for different single-walker Markov graphs G_m. Both a Barabási–Albert and a Erdős–Rényi graph are considered with row normalization (blue and orange, respectively) and without row normalization (green and red, respectively). Without row normalization, the single-walker policies Q_m are symmetric. Each curve is averaged over 10^4 simulations.

During a short time interval, the process does not have enough time to average out. Therefore, while two different symmetric walker policies can have the exact same uniform steady state, they still describe different dynamics on short timescales.

The generation of directed single-walker Markov graphs G_m using a model that generates undirected graphs, requires that the weights of the links be changed in such a way that the link $i \sim j$ generally has a different weight than the link $j \sim i$. For example, if the rates $(Q_m)_{ij}$ are divided by the degree d_i of location i in the Markov graph G_m, then $(Q_m)_{ii} = -1$ for all i and the infinitesimal generator will not be symmetric unless the Markov graph G_m is regular. We call this method *row normalization*. There are many other ways to make an undirected graph directed, such as assigning random weights or setting $(Q_m)_{ij}$ or $(Q_m)_{ji}$ (but not both) to zero for some links $i \sim j$. There is no reason to assume there is a "best" way to make a directed graph from an undirected one in general.

Figure 5 shows an experiment that investigates symmetric policies and row normalization: the maximum clique size is shown for four different CRWIG simulations with $M = 100$ walkers on Markov graphs with $N = 100$ nodes. In red and green, respectively, CRWIG is shown for walkers whose Markov graph G_m is a symmetric ER-graph and a symmetric BA-graph. In orange and blue, we show CRWIG for walkers, whose Markov graph G_m is the same ER and BA graph, but with the rows of the adjacency matrix normalized as described above. The walkers with symmetric policies have the same steady-state behavior by Theorem 9. We also observe that the difference between the normalized BA graph and the undirected BA graph is larger than the difference between the normalized ER graph and the undirected ER graph. This difference is expected because ER graphs are very regular and thus retain more symmetry after row normalization.

B. Identical walker policies: Simulation on a real-world network

As discussed in Sec. II A, when all walkers have the same policy $Q_m = Q$, CRWIG becomes equivalent to a metapopulation model and the policy Q can be interpreted as a population flow model [14]. The assumption that the walkers share a common policy Q leads to several simplifications [9]. We focus on the property that, if π is the steady-state distribution of the common policy Q, the expected fraction of walkers in location i converges to π_i. This claim follows from the observation that the number of walkers in location i in the steady state M_i is binomially distributed, because $\Pr[M_i = m] = (\pi_i)^m(1-\pi_i)^{M-m}$. The expected value follows as $E[M_i] = \pi_i M$ and here π_i is the fraction of walkers that are expected to be in location i in the steady state. Our experiment uses a train transportation network derived from data available from Ref. [24]. Our network contains 250 train stations across the Netherlands. Two stations i and j are linked if a train operated by Nederlandse Spoorwegen (Dutch Railways) departed from station i and arrived next at station j at any time during the month of April 2025. The resulting network is the common Markov graph $G = G_m$ for all walkers m. The graph is nonsymmetric and shown on the left in Fig. 6. On the right, Fig. 6 shows the number of walkers out of $M = 10^6$ walkers that are at the stations of Delft, Enschede and Maastricht over time. In black, the expected number of walkers in the locations M_{Delft}, M_{Enschede}, and $M_{\text{Maastricht}}$ are shown. These are calculated with the steady-state vector π, which is calculated by finding the left-eigenvector corresponding to eigenvalue 0 of Q. We observe that the simulation average indeed converges to the theoretical steady-state value.

C. CRWIG on geometric networks and beyond exponential times

Many statistical properties of human mobility are characterized by nonexponential distributions [3–5], which do not generally occur in Markov models. In particular, the pause-time (single-walker sojourn time) and the flight length (distance traveled per transition) for each walker, as well as the intermeeting times between walkers, have nonexponential distributions in the data. The Markovian CRWIG model can have arbitrary flight length distributions (by constructing suitable walker policies on geometric graphs) and in specific cases (e.g., on the cycle graph [5]), the Markovian model can have nonexponential intermeeting time distributions. Nonexponential pause times, however, cannot occur in the Markovian model.

In this section, we extend the Markovian CRWIG model to the non-Markovian SMRWIG model, which gives the walkers nonexponential sojourn time distributions (pause times), but keeps the same transition probabilities as the Markovian process. We then pick the single-walker policies Q_m (and thus the single-walker Markov graphs G_m) in such a way that the process also has arbitrary flight length distribution and power-law with exponential tail intermeeting times, thus showing that SMRWIG can describe contact networks generated by statistically realistic human mobility patterns.

Arbitrary walker sojourn times. For the extension of CRWIG to nonexponential sojourn times, we use a semi-Markov generalization on the single-walker level. A semi-Markov

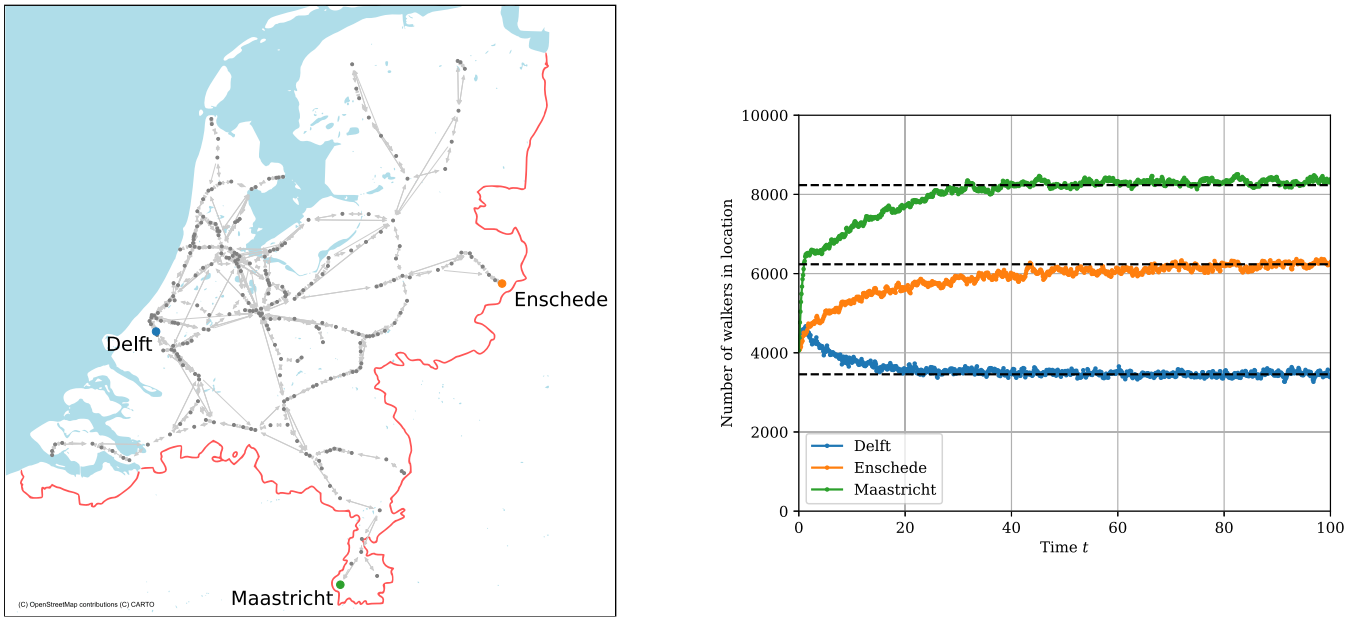

FIG. 6. (left) Map of our NS train network. (right) The number of walkers (out of $M = 10^6$) that are in three select locations: Delft (blue), Enschede (orange), and Maastricht (green). These three stations are also shown on the map in the same colors. In black are the theoretically computed values of the expected number of walkers in the three locations in the steady state. The map used is an edited version of "Positron (No Labels)" by CartoDB [25], accessed via the contextily Python package [26].

process generalizes a Markov process, defined on the same state space, with the same transition probabilities, but with a generalized sojourn time distribution, similar to the renewal process (Ref. [12], Chap. 8) that generalizes the exponential Poisson interevent times to a general distribution. In our case, the semi-Markov random walker induced temporal graph (SMRWIG) model preserves the embedded Markov chain [12,27] of the Markovian single-walker process while the single-walker sojourn times follow a general distribution $\Pr[\tau_{i,m} \leqslant t] = F_i(t;m)$ for walker m in state i. The walker m, who just arrived in state i, transitions after a time distributed as $\Pr[\tau_{i,m} > t] = 1 - F_i(t;m)$ to a specific node j with probability $\Pr[j] = \frac{(Q_m)_{ij}}{\sum_{k\neq i}(Q_m)_{ik}}$. Therefore, if $F_i(t;m) = 1 - e^{(Q_m)_{ii}t}$, the sojourn times are exponentially distributed and SMRWIG reduces to CRWIG. We emphasize that, on the ensemble level, the process is not semi-Markovian. Indeed, independent semi-Markovian walkers will generally result in ensemble sojourn times that are not memoryless, and SMRWIG is therefore a non-Markovian model.

Arbitrary flight length distributions. Flight length distributions require a node embedding in a metric space. We choose here a two-dimensional Euclidean space. We consider a particular easy topology: the *heterogeneous square lattice*, where the distance between rows and columns are distributed according to some nonconstant distribution. As an example on the left in Fig. 7, we consider a two-dimensional square Weibull lattice, where the distance between each pair of consecutive rows and each pair of consecutive columns is Weibull distributed, $F_{\text{dist}}(x) = \Pr[\text{dist} \leqslant x] = 1 - e^{-(\lambda t)^\alpha}$. A homogeneous random walk, where the next node in the random walk is one of the neighbors of the current node uniformly at random, on a "large enough" heterogeneous square lattice, has travel distances with the same distribution as the distribution of the link or column distances if enough steps are made. These properties hold in any dimension and, specifically, for the one-dimensional lattice, which is the path graph shown on the bottom right in Fig. 7. A heterogeneous path graph can (except in some pathological cases) be closed in Euclidean two-dimensional space to become a heterogeneous cycle, shown on the top right in Fig. 7. Both the two-dimensional square lattice and the cycle can generate power-law regimes of the intermeeting times as shown in the next paragraph.

Power-law with exponential tail intermeeting times. To show that our non-Markovian SMRWIG model can produce the intermeeting time power-law regime from the literature, we present some simulation results for different sojourn-time distributions in Fig. 8. Figure 8(a) shows the exact distribution of the different sojourn times and the sampled single-walker sojourn times employed in the simulation. Figure 8(a) confirms that the single walker semi-Markov correctly enforces the chosen sojourn-time distributions. Figures 8(b) and 8(c)

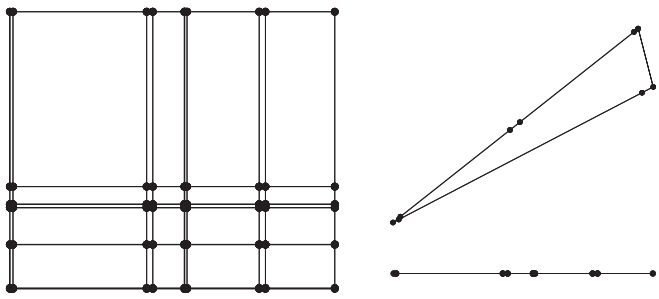

FIG. 7. Three heterogeneous lattices: on the left a two-dimensional square Weibull lattice is shown, on the right a one-dimensional square Weibull lattice and its two-dimensional closure, which is a Weibull cycle, are shown.

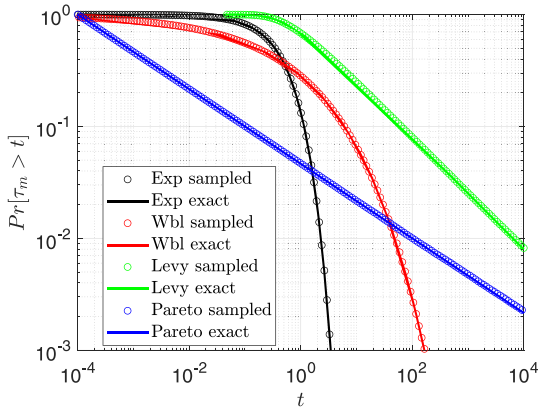

(a)

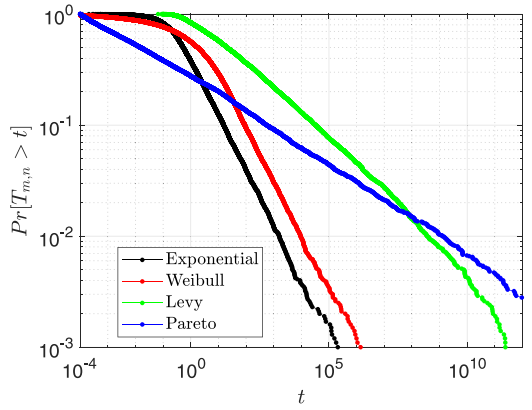

(b)

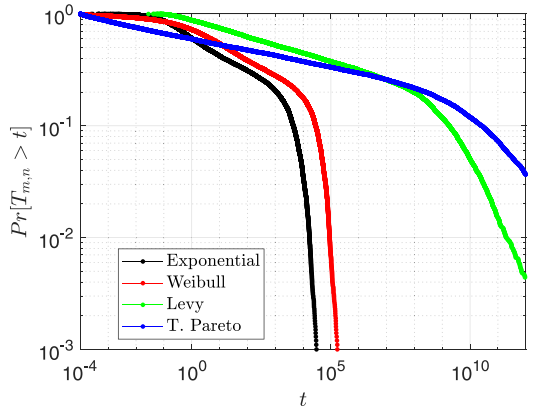

(c)

FIG. 8. Distributions from SMRWIG simulations. The simulated sojourn-time distributions are exponential $[F_i(t;m) = 1 - e^{(Q_m)_{ii}t}]$, Weibull $[F_i(t;m) = 1 - e^{-[-(Q_m)_{ii}t]^\alpha}]$, Levy $[F_i(t;m) = \text{erfc}[-(Q_m)_{ii}t]]$ and Pareto $[F_i(t;m) = 1 - (\frac{L}{x})^\alpha]$. We have chosen $\alpha = \frac{1}{3}$, $L = 10^{-4}$. In panel (a) the distribution of 10^4 sojourn times is shown for uniform walkers on the cycle graph of size $N = 10^4$. The exact equations of the distributions are thus found by substituting $(Q_m)_{ii} = -2$ for all i and m. In panel (b), for each sojourn-time distribution, the distribution of 10^4 intermeeting times is shown for uniform walkers on the cycle graph of size $N = 10^4$. In panel (c), for each sojourn-time distribution, the distribution of 10^4 intermeeting times is shown for uniform walkers on a square lattice of size $N = 10^4$.

show the power-law with exponential tail intermeeting time tail distributions, for uniform random walkers on the cycle graph [Fig. 8(b)] and on the two-dimensional square lattice [Fig. 8(c)]. We observe that the structure of the Markov graph plays a large role in the existence and slope of the power-law regime. Indeed, for most Markov graphs, the power-law regime does not exist. While changing the sojourn-time distribution can decrease the slope (make the curves flatter), it is seemingly impossible to produce a faster decreasing power law than for the exponential distribution on a given Markov graph. Fitting the walker policies and sojourn-time distributions to data (e.g., the data from Ref. [3]) is a challenging task that is beyond the scope of the current work and will be left to future research.

VI. CONCLUSION

Following the idea in Ref. [9], CRWIG describes M walkers executing independent Markov processes on the same state space, all evolving on a common global time scale. CRWIG assumes that if two or more walkers occupy the same state at time t, a link is established between them in the temporal contact graph $G(t)$. After defining a proper state numbering for the M-walker process (1), we deduce the exact infinitesimal generator of the ensemble process in (2), where a transition between two states belonging to the N^M state space is dictated by the transition rate of the individual walker that changes position. We then iteratively build the Markov graph of the CRWIG process, highlighting the multilayered structure that arises (see Fig. 2) and providing, in terms of Kronecker sums, the exact expression for both the adjacency matrix of the Markov graph and the ensemble infinitesimal generator (9).

We then consider the discretized version of the CRWIG model over successive intervals of length Δt and we obtain two main results: (1) Theorem 1 shows that under exact discretization both the ensemble Markov process and the discrete process whose transition matrix is built from the exact single-walker transition probability matrices are the same process (i.e. the processes have the same distribution at all times $k\Delta t$); (2) Theorem 2 shows that the time-sampled CRWIG model, which approximates the continuous time expanding the transition probability at first order in Δt, does not correspond to the discrete process built from the time-sampled single-walker transition probability matrices.

We discuss the fundamental differences between CRWIG and DRWIG. First, the discretized process allows transitions to happen simultaneously, which is not possible in the continuous-time formalism. This can lead to contacts that physically must happen in continuous-time not occurring in discrete time. Second, the exact discretization includes multiple hop transitions. With the one-hop interpretation of the transition probability matrix, the topology imposed for a single walker in CRWIG is lost when considering the exact discrete-time version of the model. Third, at high time resolution CRWIG is computationally superior to DRWIG, which requires each walker's transitions to be evaluated at each time step, while CRWIG only requires a walker's transitions to be evaluated after each movement.

Section IV presents various analytical results. The main results from Almasan *et al.* [9] are directly translated into continuous time (e.g., the probability of a specific contact graph G at time t). Then the decay of the influence of the initial state and the steady-state of symmetric walkers are proven for both the continuous and the discrete model. Additionally, we prove that the CRWIG process shows an exponential decay of the initial condition and exponential tail behavior of the intermeeting time distribution. Hence, in order to reproduce the heavy-tailed nature of human mobility [1,3–5], CRWIG must be extended to include nonexponential sojourn times, as shown in Theorem 8, and/or interactions between the walkers and/or memory effects.

Therefore, we propose the SMRWIG extension, which preserves the single-walker transition probabilities but with arbitrarily distributed single-walker sojourn times. SMRWIG is semi-Markovian on the single-walker level, but non-Markovian on the ensemble level. We show that SMRWIG is able to reproduce three statistical properties in agreement with human mobility data: (1) arbitrary flight length distributions due to the Markov graph (see Fig. 7); (2) arbitrary pause-time distributions [see Fig. 8(a)]; and (3) power law with exponential tail intermeeting time distributions [see Figs. 8(b) and 8(c)]. We observe that the intermeeting time distribution is primarily influenced by the Markov graph of the walkers, rather than the sojourn-time distribution.

We see several directions for future research. The Markovian formalism obtained for the CRWIG process will be the starting point to define a combined process that describes both the contact graph dynamics and the dynamics of a spreading process on top of the temporal graph. We will determine an analytical representation that describes any Markovian compartmental model (e.g., SI, SIR, SIS) on the contact network generated by the CRWIG model, and we will explore how the exact analysis of the model can be pushed forward. Additionally, we plan to apply CRWIG and the SMRWIG extension to real-world data to understand which underlying topologies and sojourn time distributions describe real-world human mobility best.

ACKNOWLEDGMENTS

We thank Brian L. Chang for his contribution of simulation results in this article. This research has been funded by the European Research Council (ERC) under the European Union's Horizon 2020 research and innovation programme (Grant Agreement No 101019718).

DATA AVAILABILITY

Some of the data that support the findings of this article are openly available [24]. The simulator used to generate our simulation results is not publicly available because it is owned by a third party and the terms of use prevent public distribution. The data are available from the authors upon reasonable request.

APPENDIX A: PROOFS

1. Proof of the transitivity claim in Sec. III C

Proof. First we show that if $(Q_m)_{ab} > 0$, then $(e^{(Q_m)t})_{ab} > 0$ for all finite $t > 0$. This follows because $(e^{(Q_m)t})_{ab} = \Pr[X_m(t) = b | X_m(0) = a] \geqslant (Q_m)_{ab} \int_0^t dx\, e^{-(Q_m)_{bb}(t-x)} e^{(Q_m)_{aa}x} > 0$, where we used the renewal equation [Ref. [12], Eq. (8.9)].

Then, since $(P_m)_{ij} > 0$ and $(P_m)_{jk} > 0$ there must be a path in the Markov graph G_m from i to k, say $z_1 = i, z_2, \ldots, z_K = k$. Each link in the Markov graph corresponds to a transition rate $(Q_m)_{z_i, z_{i+1}} > 0$ and thus we find that $(P_m)_{ik} \geqslant \prod_{i=1}^{K} \Pr[X(\frac{i\Delta t}{K}) = z_i | X(\frac{(i-1)\Delta t}{K}) = z_{i-1}] \prod_{i=1}^{K} (e^{Q\frac{\Delta t}{K}})_{z_i, z_{i+1}} > 0$ using that $(e^{Q\frac{\Delta t}{K}})_{z_i, z_{i+1}} > 0$ because $(Q_m)_{z_i, z_{i+1}} > 0$. ■

2. General proof for Sec. IV B

To prove the influence of the initial state decays exponentially also for nondiagonalizable infinitesimal generators $\mathcal{Q}$ and transition probabilities $\mathbb{P}$, we need to use Jordan forms. We first state the basic knowledge required for this proof from the book by Meyer [28].

Any $N \times N$ matrix A can be written in the Jordan form $J = BAB^{-1}$, where

$$J = \begin{bmatrix} J(\lambda_1) & 0 & \ldots & 0 \\ 0 & J(\lambda_2) & \ldots & 0 \\ \vdots & \vdots & \ddots & \vdots \\ 0 & 0 & \ldots & J(\lambda_s) \end{bmatrix},$$

where $s \leqslant N$ is the number of distinct eigenvalues and $J(\lambda_j)$ has the shape

$$J(\lambda_j) = \begin{bmatrix} J_1(\lambda_j) & 0 & \ldots & 0 \\ 0 & J_2(\lambda_j) & \ldots & 0 \\ \vdots & \vdots & \ddots & \vdots \\ 0 & 0 & \ldots & J_{t_j}(\lambda_j) \end{bmatrix},$$

where $J_i(\lambda_j)$ has the shape

$$J_i(\lambda_j) = \begin{bmatrix} \lambda_j & 1 & & \\ & \ddots & \ddots & \\ & & \ddots & 1 \\ & & & \lambda_j \end{bmatrix}.$$

Next, we state some properties related to Jordan forms from Ref. [28] that we will employ throughout this section:

(1) The sum of the sizes of the t_j blocks $J_i(\lambda_j)$ is equal to the multiplicity m_j of the eigenvalue λ_j.

(2) The largest of the $J_i(\lambda_j)$ has size $k_j \times k_j$, where k_j is called the index of the eigenvalue λ_j.

(3) Any function of a nondiagonalizable matrix A can be written as

$$f(A) = \sum_{i=1}^{s} \sum_{j=0}^{k_i - 1} f^{(j)}(\lambda_i) Z_{ij}, \tag{A1}$$

where $Z_{ij} = (A - \lambda_i I)^j G_i / j!$, where G_i, which is independent of the choice of B, is given by $G_i = B_i (B^{-1})_i$, which are defined by partitioning B and B^{-1} conformably to the partition

of J into its s Jordan segments:

$$B = [B_1 \cdots B_s], \quad J = \begin{bmatrix} J(\lambda_1) & & \\ & \ddots & \\ & & J(\lambda_s) \end{bmatrix},$$

$$B^{-1} = \begin{bmatrix} B_1^{-1} \\ \vdots \\ B_s^{-1} \end{bmatrix}.$$

(4) If the eigenvalue λ_j has multiplicity $m_j = 1$, then $k_j = 1$ and G_j is given by xy^T/y^Tx, where x and y^T are the left- and right-eigenvalues belonging to λ_j, respectively.

Discrete time. We first prove the discrete-time case. We need to assume that $\mathbb{P}$ is aperiodic and irreducible, otherwise, there is no unique steady state π reachable from every initial condition. We insert $f(\mathbb{P}) = \mathbb{P}^k$ in (A1) and find

$$\mathbb{P}^k = \sum_{i=2}^{s} \sum_{j=0}^{k_i-1} \lambda_i^{k-j} \frac{k!}{(k-j)!} Z_{ij} + \sum_{j=0}^{k_1-1} \lambda_1^{k-j} \frac{k!}{(k-j)!} Z_{1j}.$$

Because $\lambda_1 = 1$ has multiplicity one ($\mathbb{P}$ is an aperiodic irreducible stochastic matrix), it follows from properties 1 and 2 above that $1 \leqslant k_1 \leqslant m_1 = 1$ and thus we find

$$\begin{aligned} \mathbb{P}^k &= \sum_{i=2}^{s} \sum_{j=0}^{k_i-1} \lambda_i^{k-j} \frac{k!}{(k-j)!} Z_{ij} + Z_{10} \\ &= G_1 + \sum_{i=2}^{s} \sum_{j=0}^{k_i-1} \lambda_i^{k-j} \frac{k!}{(k-j)!} Z_{ij}, \end{aligned}$$

where we have substituted $Z_{10} = \frac{(\mathbb{P}-I)^0 G_i}{0!} = G_1$. It follows from property 4 that $G_1 = xy^T/y^Tx$ and since x is equal to the all-1 vector u and y^T is equal to π, we have $y^Tx = 1$ and $G_1 = u\pi$. We find that

$$\begin{aligned} \Pr[G[k] = G | X[0] = g] &= \sum_{\omega \in \Omega_G} (\mathbb{P}^k)_{gi} \\ &= \sum_{\omega \in \Omega_G} \pi_\omega + \sum_{i=2}^{s} \sum_{j=0}^{k_i-1} \lambda_i^{k-j} \frac{k!}{(k-j)!} (Z_{ij})_{g\omega}, \end{aligned} \tag{A2}$$

where all terms in the second sum decay exponentially in k, because $|\lambda_i| < 1$, for $i > 1$ ($\mathbb{P}$ is aperiodic and irreducible) and the factorial terms are a polynomial of order j, which is bounded by $k_i - 1 \leqslant M^N$.

Continuous time. Similarly, in the continuous-time case, we need to assume that the steady state is unique. Under this assumption, the Markov graph has a single strongly connected component, which is reachable from every node. A unique steady state implies that the multiplicity m_1 of the eigenvalue $\lambda_1 = 0$ of $\mathcal{Q}$ is equal to one. We insert $f(\mathcal{Q}) = e^{\mathcal{Q}t}$ in (A1) to find

$$e^{\mathcal{Q}t} = \sum_{i=2}^{s} \sum_{j=0}^{k_i-1} e^{\lambda_i t} t^j Z_{ij} + e^{\lambda_1 t} Z_{10},$$

where, as with $\mathbb{P}$, the eigenvalue $\lambda_1 = 0$ has multiplicity one, such that only the term where $j = 0$ contributes. Additionally, the eigenvectors of λ_1 are the same as for $\mathbb{P}$ above, so we find

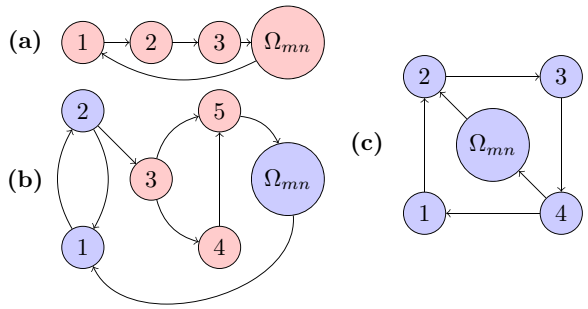

FIG. 9. Three Markov graphs illustrating deterministic (red) and nondeterministic nodes (blue). From each deterministic node, every walk is a path until a node in Ω_{mn} is reached. In panel (a) node Ω_{mn} is deterministic, while in panels (b) and (c) Ω_{mn} is nondeterministic. Additionally, panels (a) and (c) illustrate that the longest deterministic path and the longest path from a nondeterministic node to Ω_{mn} contain at most the number of nodes N in the Markov graph.

completely analogous to the discrete case that

$$\begin{aligned} e^{\mathcal{Q}t} &= \sum_{i=2}^{s} \sum_{j=0}^{k_i-1} e^{\lambda_i t} t^j Z_{ij} + e^{\lambda_1 t} Z_{10} \\ &= G_1 + \sum_{i=2}^{s} \sum_{j=0}^{k_i-1} e^{\lambda_i t} t^j Z_{ij} \\ &= u\pi + \sum_{i=2}^{s} \sum_{j=0}^{k_i-1} e^{\lambda_i t} t^j Z_{ij}. \end{aligned}$$

Thus, since $(u\pi)_{ij} = \pi_j$ we find

$$\begin{aligned} \Pr[G(t) = G | X(0) = g] &= \sum_{\omega \in \Omega_G} (e^{\mathcal{Q}t})_{g\omega} \\ &= \sum_{\omega \in \Omega_G} \pi_\omega + \sum_{i=2}^{s} \sum_{j=0}^{k_i-1} e^{\lambda_i t} t^j (Z_{ij})_{g\omega}, \end{aligned} \tag{A3}$$

where the second sum decays exponentially because all $\lambda_i > 1$ have negative real part [12], and j is bounded from above by $k_i - 1 \leqslant M^N$. While the second sum in both the discrete-time case (A2) and the continuous-time case (A3) decays exponentially, this decay can still be very slow. If some $|\lambda_i|$ are close to 1, the decay of λ_i^k is slow in the discrete case, and, similarly, if the real part of λ_i is only slightly below zero in the continuous case, the decay of $e^{\lambda_i t}$ is slow. Additionally, if the eigen-structure is particularly degenerate, the polynomials in j that are present in the second sum in (A2) and (A3) can be of high order, slowing down the decay as well.

3. Proof of Lemma 6

Proof. We introduce the concept of *deterministic nodes*. The deterministic nodes of the two-walker Markov graph are those nodes that have the property that every walk starting in one of them is a path until a node from Ω_{mn} is reached. Since paths do not contain cycles, this means a cycle cannot be reached from a deterministic node without first reaching a node in Ω_{mn}. In Fig. 9 the deterministic nodes are shown in red. The nodes that are not deterministic are called *nondeter-*

ministic nodes, shown in blue in Fig. 9. Figure 9 illustrates that nodes in Ω_{mn} can be both deterministic and nondeterministic, depending on the structure of the Markov graph. The most important property of deterministic nodes for our purposes is that from any deterministic node, we reach a state in Ω_{mn} in less than N^2 steps with probability one. This follows directly because $\mathcal{Q}_2$ has N^2 states and the longest path on N^2 nodes has length N^2. This bound is very loose, since $|\Omega_{mn}| = N$ and long path structures are not possible in $\mathcal{G}_2$ due to the walker independence.

We prove Lemma 6 by considering two cases: $l(W) \leqslant 2N^2$ and $l(W) > 2N^2$. We construct our exponential upper bound such that it is larger than one for $k \leqslant 2N^2$. Then, the upper bound on $\Pr[l(W) = k]$ holds trivially for those values of k and we only need to consider the case $l(W) > 2N^2$. If $l(W)$ is $k = N^2 + s$, at least the first s nodes of the walk W must be nondeterministic, since the maximum number of deterministic nodes in W is N^2. It is possible that from some set of (nondeterministic) nodes S, no nodes from Ω_{mn} can be reached. When considering intermeeting walks W, no nodes from S can be part of W since W is inherently conditioned on reaching Ω_{mn} after $l(W) - 1$ steps. Therefore, we remove the nodes in S from our consideration without loss of generality and assume that Ω_{mn} can be reached from any node in $\mathcal{G}_2$, which requires that there has to be at least one path with nonzero probability to a node in Ω_{mn} from each nondeterministic node. The longest of such paths has length at most N^2. Therefore, the probability of staying in nondeterministic nodes for N^2 steps can be bounded from above by some $p < 1$ independent of which nondeterministic node the first step is taken from. Then, the probability of staying in nondeterministic states for s steps can be upper-bounded by[1] $p^{\lfloor \frac{s}{N^2} \rfloor}$ if $s > N^2$. Thus, for $k > 2N^2$ we find that

$$\begin{aligned}
&\Pr[l(W) = k] \\
&\quad \leqslant \Pr[W \text{ contains } k - N^2 \text{ nondeterministic nodes}] \\
&\quad \leqslant p^{\lfloor \frac{k-N^2}{N^2} \rfloor} \leqslant p^{\frac{k-N^2}{N^2} - 1}
\end{aligned}$$

and because $\frac{k-N^2}{N^2} - 1 \leqslant 0$ for $k \leqslant 2N^2$, the bound $p^{\frac{k-N^2}{N^2}-1} \geqslant 1$ for $k \leqslant 2N^2$ and is thus valid for all k. After rewriting:

$$p^{\frac{k-N^2}{N^2}-1} = p^{\frac{k}{N^2}-2} = \frac{1}{p^2} p^{\frac{k}{N^2}} = C e^{\frac{\ln(p)}{N^2} k} = C e^{-ak},$$

where $\ln(p) = -aN^2$ for some real, finite $a > 0$ since $0 < p < 1$ and Lemma 6 is proven. ■

4. Proof of Theorem 7

Proof. We apply the law of total probability, conditioned on the length (number of states) $l(W)$ of the intermeeting walk W the two-walker process performs before the walkers meet again:

$$\begin{aligned}
\Pr[T_{m,n} > x] &= \sum_{k=2}^{\infty} \Pr[l(W) = k] \Pr[T_{m,n} > x | l(W) = k] \\
&= \sum_{k=2}^{\infty} \Pr[l(W) = k](1 - \Pr[T_{m,n} \leqslant x | l(W) = k]).
\end{aligned}$$

We now condition the probability $\Pr[T_{m,n} \leqslant x | l(W) = k]$ on all intermeeting walks $\tilde{w} \in W_k$, where W_k is the set of intermeeting walks of length k. The condition on $\tilde{w}$ and $l(W) = k$ simplifies to a condition on only $\tilde{w}$ since $\tilde{w}$ has length k and with the law of total probability, we find

$$\begin{aligned}
&\Pr[T_{m,n} > x] \\
&\quad = \sum_{k=2}^{\infty} \Pr[l(W) = k] \\
&\qquad \times \left(1 - \sum_{\tilde{w} \in W_k} \Pr[\tilde{w} | l(W) = k] \Pr[T_{m,n} \leqslant x | \tilde{w}]\right) \\
&\quad = \sum_{k=2}^{\infty} \Pr[l(W) = k] \\
&\qquad \times \left(1 - \sum_{\tilde{w} \in W_k} \Pr[\tilde{w} | l(W) = k] \Pr\left[\sum_{i=1}^{k-1} T_{\tilde{w}_i, \tilde{w}_{i+1}} \leqslant x\right]\right) \\
&\quad = \sum_{k=2}^{\infty} \Pr[l(W) = k] \\
&\qquad \times \sum_{\tilde{w} \in W_k} \Pr[\tilde{w} | l(W) = k] \left(1 - \Pr\left[\sum_{i=1}^{k-1} T_{\tilde{w}_i, \tilde{w}_{i+1}} \leqslant x\right]\right),
\end{aligned} \tag{A4}$$

where $k - 1 = l(W) - 1$ is the number of transitions in the walk $\tilde{w}$ and $T_{\tilde{w}_i, \tilde{w}_{i+1}}$ is the random time it takes to transition from $\tilde{w}_i$ to $\tilde{w}_{i+1}$, which is exponentially distributed with rate $(\mathcal{Q}_2)_{\tilde{w}_i, \tilde{w}_{i+1}} \geqslant \Theta$. Therefore, the probability $\Pr[\sum_{i=1}^{k-1} T_{\tilde{w}_i, \tilde{w}_{i+1}} \leqslant x]$ is lower bounded by the probability $\Pr[\sum_{i=1}^{k-1} Y(\Theta) \leqslant x]$, where $Y(\Theta)$ is exponentially distributed with rate Θ. Indeed Θ is the smallest rate in the infinitesimal generator and therefore the random variable $Y(\Theta)$ has the same distribution as the largest sojourn time in the Markov chain. The sum $\sum_{i=1}^{k-1} Y(\Theta)$ is distributed as an Erlang distribution [12, p.45] with shape parameter $k - 1$ and rate Θ; therefore, $\Pr[\sum_{i=1}^{k-1} Y(\Theta) \leqslant x] = F_{\text{Erlang}}(x; k-1, \Theta) = 1 - \sum_{r=0}^{k-2} \frac{1}{r!} e^{-\Theta x} (\Theta x)^r$. Applying these arguments to (A4),

[1] The floor function is defined as $\lfloor x \rfloor = n$ where n is the largest integer such that $n \leqslant x$.

we find

$$\begin{aligned}\Pr[T_{m,n} > x] &= \sum_{k=2}^{\infty} \Pr[l(W) = k] \sum_{\tilde{w}\in W_k} \Pr[\tilde{w}|l(W) = k]\left(1 - \Pr\left[\sum_{i=1}^{k-1} T_{\tilde{w}_i,\tilde{w}_{i+1}} \leqslant x\right]\right)\\ &\leqslant \sum_{k=2}^{\infty} \Pr[l(W) = k] \sum_{\tilde{w}\in W_k} \Pr[\tilde{w}|l(W) = k]\left(1 - \Pr\left[\sum_{i=1}^{k-1} Y(\Theta) \leqslant x\right]\right)\\ &= \sum_{k=2}^{\infty} \Pr[l(W) = k]\left[1 - F_{\text{Erlang}}(x; k-1, \Theta)\right]\\ &= \sum_{k=2}^{\infty} \Pr[l(W) = k] \sum_{r=0}^{k-2} \frac{1}{r!} e^{-\Theta x}(\Theta x)^r.\end{aligned}$$

We substitute the result from Lemma 6 and reverse the order of summation:

$$\begin{aligned}\Pr[T_{m,n} > x] &\leqslant \sum_{k=2}^{\infty} Ce^{-ak} \sum_{r=0}^{k-2} \frac{1}{r!} e^{-\Theta x}(\Theta x)^r = \sum_{r=0}^{\infty} \sum_{k=r+2}^{\infty} Ce^{-ak} \frac{1}{r!} e^{-\Theta x}(\Theta x)^r\\ &= Ce^{-\Theta x} \sum_{r=0}^{\infty} \left(\sum_{k=r+2}^{\infty} e^{-ak}\right) \frac{1}{r!}(\Theta x)^r = Ce^{-\Theta x} \sum_{r=0}^{\infty} \left(\frac{e^{-a(r+1)}}{e^a - 1}\right) \frac{1}{r!}(\Theta x)^r\\ &= C\frac{e^{-a}}{e^a - 1} e^{-\Theta x} \sum_{r=0}^{\infty} \frac{e^{-ar}}{r!}(\Theta x)^r = C\frac{1}{e^a(e^a - 1)} e^{-\Theta x} e^{\Theta x e^{-a}}. \qquad \text{(A5)}\end{aligned}$$

Hence, we arrive at

$$\Pr[T_{m,n} > x] \leqslant C\frac{1}{e^a(e^a - 1)} e^{-(1-e^{-a})\Theta x} = \tilde{C}e^{-(1-\xi)\Theta x},$$

where $\tilde{C} < \infty$ and $0 < \xi = e^{-a} < 1$, which completes the proof. ■

APPENDIX B: RESTRICTION TO A GRAPH G

To keep the model as general as possible, we allowed the walker policies Q_m to be the Laplacian of any single-walker Markov graph G_m with node set $\mathcal{N}$. In real-world scenarios, we may be interested in a situation in which walkers are restricted to move on an underlying graph G, instead of the unrestricted vertex set. Then, not every policy Q_m will be possible because the single-walker Markov graph G_m may contain a link between two nodes i and j that are not connected in the underlying graph G.

The walkers in CRWIG can be restricted to an underlying graph G, by imposing that G_m cannot have links other than the ones in G. We still allow the links to be weighted and nonsymmetric as in the general case. The underlying graph G determines which links do not exist but not their weights. To restrict the walker policy Q_m only to the links in G, we remove the links from node i to node j in G_m if there is no link from i to j in G. We write $G_m(G)$ for the mth walker single-walker Markov graph G_m restricted to G and $A_m(G)$ for its adjacency matrix. We obtain

$$A_m(G) = A \circ A_m, \qquad \text{(B1)}$$

where $\circ$ indicates the Hadamard (or element-wise) product and A is the adjacency matrix of the unweighted underlying graph G. The elements $(A_m(G))_{ij}$ are equal to $(A_m)_{ij}a_{ij} = (A_m)_{ij}\mathbf{1}_{i\sim j}$, where the indicator function $\mathbf{1}_{i\sim j}$ is 1 if there is a link from i to j in G and 0 otherwise. The restricted walker policy $Q_m(G)$ is then again minus the Laplacian of the restricted single-walker Markov graph $G_m(G)$. We emphasize that not all walkers have to be restricted in this setting. Additionally, different walkers can be given different restrictions. This could, for example, correspond to a traffic network where some walkers are using public transport, some are driving a car, and some are on foot. Each of these groups could then be restricted to a different underlying graph on the same vertex set $\mathcal{N}$. Restricting all walkers to the same underlying graph G is equivalent to the base case in the original discrete RWIG model [9].

APPENDIX C: BLOCK MATRIX STRUCTURE OF STATE TRANSITIONS

It follows from construction that the index of the matrices are in agreement with (1). Each walker added per iteration step corresponds to adding a digit in front of the base N representation of the state (e.g., $x_3x_2x_1$ becomes $x_4x_3x_2x_1$). The base-N state numbering (1) orders the states as

$$1111, \ldots, 1NNN, 2111, \ldots 2NNN, 3111, \ldots, NNNN.$$

Each possible configuration of walkers 1, 2, and 3 with walker 4 in state 1 comes before each possible configuration of walkers 1, 2, and 3 with walker 4 in state 2, and so on. This is the reason for the block structure of the iterative process of adding walkers. See, for example, the case below, which extends a system with 2 walkers on two nodes to 3 walkers on two nodes. The elements $x_2(i)x_1(i), x_2(j)x_1(j)$ indicate

the transitions from state $x_2(i)x_1(i)$ to state $x_2(j)x_1(j)$. The four blocks correspond to walker 3 moving from the node indicated on the left of the block to the node indicated at the top. When this transition is added to the base-N state numbering $x_3(i)x_2(i)x_1(i), x_3(j), x_2(j), x_1(j)$, it can be seen that the enumeration order is preserved.

$$
\begin{array}{c|cc}
 & 1 & 2 \\
1 & \begin{bmatrix} 11,11 & 11,12 & 11,21 & 11,22 \\ 12,11 & 12,12 & 12,21 & 12,22 \\ 21,11 & 21,12 & 21,21 & 21,22 \\ 22,11 & 22,12 & 22,21 & 22,22 \end{bmatrix} & \begin{bmatrix} 11,11 & 11,12 & 11,21 & 11,22 \\ 12,11 & 12,12 & 12,21 & 12,22 \\ 21,11 & 21,12 & 21,21 & 21,22 \\ 22,11 & 22,12 & 22,21 & 22,22 \end{bmatrix} \\
2 & \begin{bmatrix} 11,11 & 11,12 & 11,21 & 11,22 \\ 12,11 & 12,12 & 12,21 & 12,22 \\ 21,11 & 21,12 & 21,21 & 21,22 \\ 22,11 & 22,12 & 22,21 & 22,22 \end{bmatrix} & \begin{bmatrix} 11,11 & 11,12 & 11,21 & 11,22 \\ 12,11 & 12,12 & 12,21 & 12,22 \\ 21,11 & 21,12 & 21,21 & 21,22 \\ 22,11 & 22,12 & 22,21 & 22,22 \end{bmatrix}
\end{array}
$$

$$
= \begin{bmatrix}
111,111 & 111,112 & 111,121 & 111,122 & 111,211 & 111,212 & 111,221 & 111,222 \\
112,111 & 112,112 & 112,121 & 112,122 & 112,211 & 112,212 & 112,221 & 112,222 \\
121,111 & 121,112 & 121,121 & 121,122 & 121,211 & 121,212 & 121,221 & 121,222 \\
122,111 & 122,112 & 122,121 & 122,122 & 122,211 & 122,212 & 122,221 & 122,222 \\
211,111 & 211,112 & 211,121 & 211,122 & 211,211 & 211,212 & 211,221 & 211,222 \\
212,111 & 212,112 & 212,121 & 212,122 & 212,211 & 212,212 & 212,221 & 212,222 \\
221,111 & 221,112 & 221,121 & 221,122 & 221,211 & 221,212 & 221,221 & 221,222 \\
222,111 & 222,112 & 222,121 & 222,122 & 222,211 & 222,212 & 222,221 & 222,222
\end{bmatrix}
$$

APPENDIX D: TENSOR FORMULATION OF THE MULTIWALKER PROCESS

In Sec. II, we have described the structure of the $N^M \times N^M$ Markov graph adjacency matrix $\mathcal{A}$ in (6) and of the $N^M \times N^M$ infinitesimal generator $\mathcal{Q}$ in (8). Instead of working in the matrix space $\mathbb{R}^{N^M \times N^M}$, we can reformulate the adjacency matrix $\mathcal{A}$ and the infinitesimal generator $\mathcal{Q}$ as rank-$2M$ tensors in the $\mathbb{R}^{\overbrace{N \times N \times \cdots \times N}^{2M \text{ times}}}$ space. A similar approach has been presented in (Ref. [29], Sec. 2.2) and has been employed for the hitting times calculations in Ref. [30]. We consider the tensor formulation, because it can lead to significant computational advantages [31–33]. First, due to the nice structure of our process, the tensors can be stored more efficiently in memory (MN^2 versus N^{2M}). Secondly, tensor operations can be applied more efficiently on the rank-$2M$ tensor than equivalent matrix operations on the $N^M \times N^M$ matrix.

To write the $N^M \times N^M$ matrices in tensor form, we first define as in Ref. [31], Sec. B the outer product $\square$ between two tensors as a generalization of the Kronecker product $\otimes$ between two vectors. Given a column vector $v \in \mathbb{R}^{n_1}$ and a row vector $w^T \in \mathbb{R}^{n_2}$, their Kronecker product $v \otimes w^T$ is an $n_1 \times n_2$ matrix. Similarly, given a tensor $B \in \mathbb{R}^{n_1 \times n_2 \times n_3}$ and a tensor $C \in \mathbb{R}^{d_1 \times d_2 \times d_3}$, their outer product $B \square C$ is a $n_1 \times n_2 \times n_3 \times d_1 \times d_2 \times d_3$ tensor. In particular, the element of the outer product tensor is

$$(B \square C)_{i_1 i_2 i_3 j_1 j_2 j_3} = B_{i_1 i_2 i_3} C_{j_1 j_2 j_3}. \tag{D1}$$

The tensors in the $\mathbb{R}^{\overbrace{N \times N \times \cdots \times N}^{2M \text{ times}}}$ space have the same elements as the matrices $\mathcal{A}$ and $\mathcal{Q}$. We define the tensor representations $T_{\mathcal{Q}}$ and $T_{\mathcal{A}}$ of the multiwalker infinitesimal generator $\mathcal{Q}$ and the adjacency matrix $\mathcal{A}$ of its Markov graph by assigning the elements of $\mathcal{Q}$ and $\mathcal{A}$, respectively:

$$(T_{\mathcal{Q}})_{x_1(i)x_1(j)x_2(i)x_2(j)\ldots x_M(i)x_M(j)} = \mathcal{Q}_{ij}, \tag{D2}$$

$$(T_{\mathcal{A}})_{x_1(i)x_1(j)x_2(i)x_2(j)\ldots x_M(i)x_M(j)} = \mathcal{A}_{ij}. \tag{D3}$$

We consider the multiwalker infinitesimal generator $\mathcal{Q}$ first. Ignoring the diagonal, there is some m with $x_m(i) \neq x_m(j)$ and the tensor element

$$(T_{\mathcal{Q}})_{x_1(i)x_1(j)x_2(i)x_2(j)\ldots x_M(i)x_M(j)} = (\mathcal{Q}_m)_{x_m(i)x_m(j)}$$

if, for all $k \neq m$, we have $x_k(i) = x_k(j)$ and zero otherwise [see (2)]. Using the tensor outer product (D1), we can write the tensor infinitesimal generator $T_{\mathcal{Q}}$ as

$$T_{\mathcal{Q}} = \sum_{m=1}^{M} \underbrace{I \square \cdots \square \overbrace{Q_m}^{m\text{th position}} \square \cdots \square I}_{M \text{ terms}}, \tag{D4}$$

where I is the $N \times N$ identity matrix. We consider an element from $T_{\mathcal{Q}}$ defined in (D4). There are three cases: First, the case where one walker k changes state [i.e., $x_k(i) \neq x_k(j)$, but $x_m(i) = x_m(j)$ for all $m \neq k$]. Second, the case where multiple walkers, including walkers k and l change state [i.e., $x_k(i) \neq x_k(j)$ and $x_l(i) \neq x_l(j)$]. Lastly, there is the case where no walkers change state (the diagonal elements). We show that in each case, (D2) holds.

Case 1: One walker moves. When one walker k changes state, then $x_k(i) \neq x_k(j)$, but $x_m(i) = x_m(j)$ for all other walkers $m \neq k$. Looking at the terms of the sum in (D4), all terms $m \neq k$ are zero, because in the kth place there is an identity I. The value of the chain of outer products is the product of the entries $I_{x_1(i),x_1(j)} \times \cdots \times I_{x_{m-1}(i),x_{m-1}(j)} \times (\mathcal{Q}_m)_{x_m(i),x_m(j)} \times I_{x_{m+1}(i),x_{m+1}(j)} \times \cdots \times I_{x_M(i),x_M(j)}$, which is zero when there is an identity in the kth place since $x_k(i) \neq x_k(j)$.

The remaining term has the value $(Q_k)_{x_k(i)x_k(j)}$, in agreement with (2).

Case 2: Multiple walkers move. When multiple walkers change state, then, for at least some k and some $l \neq k$, we have $x_k(i) \neq x_k(j)$ and $x_l(i) \neq x_l(j)$. With the same argument as in case 1, we find that all terms $m \neq k$ in the sum are zero, and also all terms $m \neq l$ in the sum are zero. This means the element of $T_{\mathcal{Q}}$ is zero, similar to the one in $\mathcal{Q}$, because multiple transitions are not possible at the same time in a continuous-time Markov process [12].

Case 3: No walkers move. When no walkers move, the tensor element $(T_{\mathcal{Q}})_{x_1(i)x_1(i)x_2(i)x_2(i)\ldots x_M(i)x_M(i)} = \mathcal{Q}_{ii}$ corresponds to a diagonal element of the multiwalker infinitesimal generator. This time, each term of the sum in (D4) contributes, and the sum reduces to $\sum_{m=1}^{M}(Q_m)_{x_m(i)x_m(i)}$, which is in agreement with (2).

The adjacency matrix $\mathcal{A}$ of the multiwalker Markov graph $\mathcal{G}$ can be expressed in a similar form:

$$T_{\mathcal{A}} = \sum_{m=1}^{M} \underbrace{I\square\cdots\square \overbrace{A_m}^{m\text{th position}} \square\cdots\square I}_{M \text{ terms}}. \tag{D5}$$

In order to use the tensor representation to describe or simulate the evolution of the CRIWG in time, we require a tensor equivalent of the operator $e^{\mathcal{Q}t}$ and a tensor equivalent of the state vector $s(t)$. We start with the former and write, using Theorem 1 and (15), that

$$e^{\mathcal{Q}t} = \mathcal{P}(t) = \mathbb{P}(t) = \bigotimes_{m=M}^{1} e^{Q_m t},$$

such that the elements can be written as

$$(e^{\mathcal{Q}t})_{ij} = (\mathcal{P}(t))_{ij} = \prod_{m=1}^{M} (e^{Q_m t})_{x_m(i),x_m(j)}. \tag{D6}$$

If we define the exponential of the tensor $T_{\mathcal{Q}}t$ as the tensor whose elements are

$$(e^{T_{\mathcal{Q}}t})_{x_1(i)x_1(j)x_2(i)x_2(j)\ldots x_M(i)x_M(j)} = (e^{\mathcal{Q}t})_{ij},$$

then, from (D6) and the definition of the tensor outer product (D1), it follows that the tensor $e^{T_{\mathcal{Q}}t}$ can also be written as

$$e^{T_{\mathcal{Q}}t} = \bigsquare_{m=1}^{M} e^{Q_m t}. \tag{D7}$$

We then define the tensor $T_{s(t)}$, corresponding to the state vector $s(t)$ of the N^M multiwalker process, as an $N \times N \times \cdots \times N$ rank-M tensor with elements

$$(T_{s(t)})_{x_1(i),x_2(i),\ldots,x_M(i)} = (s(t))_i = \prod_{m=1}^{M} (s_m(t))_{x_m(i)}, \tag{D8}$$

where we used (5). Using the definition of the tensor outer product (D1) it follows that:

$$T_{s(t)} = \bigsquare_{m=1}^{M} s_m(t) = \bigsquare_{m=1}^{M} s_m(0) e^{Q_m t}. \tag{D9}$$

The evolution of the multiwalker process can also be written in terms of the tensor contraction operation $\times_{[i_1,j_1],[i_2,j_2],\ldots,[i_k,j_k]}$ as defined in Ref. [31], Sec. B. The tensor contraction operator is a generalization of the vector matrix product for tensors. The subscript indicates which pairs of indices $[i, j]$ of the two tensors are contracted. Consider two tensors $A \in \mathbb{R}^{N\times N\times\cdots\times N}$ and $B \in \mathbb{R}^{N\times N\times\cdots\times N}$ of rank R_A and R_B, respectively. The contraction operator $\times_{[a_i,b_j]}$ is defined by the elements of $C = A \times_{[a_i,b_j]} B$:

$$C_{a_1,\ldots,a_{i-1},a_{i+1},\ldots,a_{R_A},b_1,\ldots,b_{j-1},b_{j+1},\ldots,b_{R_B}} = \sum_{n=1}^{N} A_{a_1,\ldots a_{i-1},n,a_{i+1},\ldots,a_{R_A}} B_{b_1,\ldots b_{j-1},n,b_{j+1},\ldots,b_{R_B}}.$$

For another example, consider the two $N \times N$ matrices M_1 and M_2. The contraction operator $\times_{[2,1]}$ is the well-known matrix product: $(M_1M_2)_{ij} = \sum_{n=1}^{N}(M_1)_{in}(M_2)_{nj} = M_1 \times_{[2,1]} M_2$. If the contraction operator contracts multiple pairs, additional sums are added. The contraction operator $\times_{[a_i,b_j],[a_k,b_l]}$, when $i < k, j > l$, is defined by the elements of $C = A \times_{[a_i,b_j],[a_k,b_l]} B$:

$$C_{a_1,\ldots,a_{i-1},a_{i+1},\ldots,a_{k-1},a_{k+1},\ldots,a_{R_A},b_1,\ldots,b_{l-1},b_{l+1},\ldots,b_{j-1},b_{j+1},\ldots,b_{R_B}} = \sum_{n_1=1}^{N}\sum_{n_2=1}^{N} A_{a_1,\ldots a_{i-1},n_1,a_{i+1},\ldots a_{k-1},n_2,a_{k+1},\ldots,a_{R_A}} \times B_{b_1,\ldots b_{l-1},n_2,b_{l+1},\ldots b_{j-1},n_1,b_{j+1},\ldots,b_{R_B}}.$$

The step to contracting more than two pairs is analogous to the step from contracting one pair to contracting two pairs. Each additional contracted pair of indices adds an additional sum over all equal values of those indices. With the tensor contraction operator, the tensor state vector $T_{s(t)}$ in terms of the tensor exponent $e^{T_{\mathcal{Q}}t}$ is

$$T_{s(t)} = T_{s(0)} \times e^{T_{\mathcal{Q}}t}, \tag{D10}$$

where we write $\times$ as an abbreviation of $\times_{[1,1],[2,3],\ldots,[k,2k-1],\ldots,[M,2M-1]}$. The elements are given by:

$$(T_{s(t)})_i = \sum_{x_1(j)=1}^{N}\sum_{x_2(j)=1}^{N}\cdots\sum_{x_M(j)=1}^{N} (T_{s(0)})_{x_1(j),x_2(j),\ldots,x_M(j)} \times (e^{T_{\mathcal{Q}}t})_{x_1(j)x_1(i)x_2(j)x_2(i)\ldots x_M(j)x_M(i)},$$

where we now denote the summation indices as $x_m(j)$, to illustrate the equivalence with the nontensor form

$$(s(t))_i = \sum_{j=1}^{N^M} (s(0))_j (e^{\mathcal{Q}t})_{ji}.$$

Since the tensor state vector $T_{s(t)}$ is the tensor equivalent of the N^M state space probability vector $s(t)$, which solves the Chapman-Kolmogorov equation defining the multiwalker Markov process, Eq. (D10) can be interpreted as the tensor form of the Chapman-Kolmogorov equation (4). The tensor representation allows for the direct computation of the exact M-walker ensemble state vector from the single-walker processes in Eq. (D9). This is a very tedious operation with the $N^M \times 1$ state vector $s(t)$, due to the enumeration of the M-walker states.

[1] M. C. Gonzalez, C. A. Hidalgo, and A.-L. Barabási, Understanding individual human mobility patterns, Nature (London) **453**, 779 (2008).

[2] C. Song, T. Koren, P. Wang, and A.-L. Barabási, Modelling the scaling properties of human mobility, Nat. Phys. **6**, 818 (2010).

[3] A. Chaintreau, P. Hui, J. Crowcroft, C. Diot, R. Gass, and J. Scott, Impact of human mobility on opportunistic forwarding algorithms, IEEE Trans. Mob. Comput. **6**, 606 (2007).

[4] I. Rhee, M. Shin, S. Hong, K. Lee, S. J. Kim, and S. Chong, On the Levy-walk nature of human mobility, IEEE/ACM Trans. Networking **19**, 630 (2011).

[5] T. Karagiannis, J.-Y. Le Boudec, and M. Vojnović, Power law and exponential decay of inter contact times between mobile devices, in *Proceedings of the 13th Annual ACM International Conference on Mobile Computing and Networking* (ACM Press, New York, NY, 2007), pp. 183–194.

[6] H. Barbosa, M. Barthelemy, G. Ghoshal, C. R. James, M. Lenormand, T. Louail, R. Menezes, J. J. Ramasco, F. Simini, and M. Tomasini, Human mobility: Models and applications, Phys. Rep. **734**, 1 (2018).

[7] M. U. G. Kraemer, C.-H. Yang, B. Gutierrez, C.-H. Wu, B. Klein, D. M. Pigott, Open COVID-19 Data Working Group, L. du Plessis, N. R. Faria, R. Li, W. P. Hanage, J. S. Brownstein, M. Layan, A. Vespignani, H. Tian, C. Dye, O. G. Pybus, and S. V. Scarpino, The effect of human mobility and control measures on the COVID-19 epidemic in China, Science **368**, 493 (2020).

[8] G. Cencetti, G. Santin, A. Longa, E. Pigani, A. Barrat, C. Cattuto, S. Lehmann, M. Salathe, and B. Lepri, Digital proximity tracing on empirical contact networks for pandemic control, Nat. Commun. **12**, 1655 (2021).

[9] A.-D. Almasan, S. Shvydun, I. Scholtes, and P. Van Mieghem, Generating temporal contact graphs using random walkers, IEEE Trans. Netw. Sci. Eng. **12**, 1649 (2025).

[10] M. Génois and A. Barrat, Can co-location be used as a proxy for face-to-face contacts? EPJ Data Sci. **7**, 1 (2018).

[11] L. Alessandretti, U. Aslak, and S. Lehmann, The scales of human mobility, Nature (London) **587**, 402 (2020).

[12] P. Van Mieghem, *Performance Analysis of Complex Networks and Systems* (Cambridge University Press, Cambridge, UK, 2014).

[13] P. Van Mieghem, *Graph Spectra for Complex Networks*, 2nd ed. (Cambridge University Press, Cambridge, UK, 2023).

[14] N. Masuda and R. Lambiotte, *A Guide to Temporal Networks*, 2nd ed. (World Scientific, Singapore, 2020).

[15] P. Van Mieghem, J. Omic, and R. Kooij, Virus spread in networks, IEEE/ACM Trans. Networking **17**, 1 (2008).

[16] M. A. Achterberg and P. Van Mieghem, Analytic solution of Markovian epidemics without re-infections on heterogeneous networks, arXiv:2311.16721.

[17] NordNordWest, Netherlands relief location map, https://en.m.wikipedia.org/wiki/File:Netherlands_relief_location_map.svg, n.d, Image licensed under Creative Commons by-sa-3.0 de.

[18] N. J. Higham, *Functions of Matrices: Theory and Computation* (SIAM, Philadelphia, PA, 2008).

[19] A. P. Riascos and D. P. Sanders, Mean encounter times for multiple random walkers on networks, Phys. Rev. E **103**, 042312 (2021).

[20] S. Shvydun, A.-D. Almasan, and P. Van Mieghem, Temporal graph reproduction with RWIG, IEEE Trans. Netw. Sci. Eng. **12**, 3015 (2025).

[21] Centers for Disease Control (CDC *et al.*), Imported measles with subsequent airborne transmission in a Pediatrician's office–Michigan, Morbidity and Mortality Weekly Report (MMWR) **32**, 401 (1983).

[22] M. Alsved, K. Nyström, S. Thuresson, D. Nygren, M. Patzi-Churqui, T. Hussein, C.-J. Fraenkel, P. Medstrand, and J. Löndahl, Infectivity of exhaled SARS-CoV-2 aerosols is sufficient to transmit COVID-19 within minutes, Sci. Rep. **13**, 21245 (2023).

[23] J. C. Pringle, Covid-19 in a correctional facility employee following multiple brief exposures to persons with COVID-19—Vermont, July–August 2020, MMWR. Morbidity and Mortality Weekly Report **69**, 1569 (2020).

[24] R. de Treinen, Train archive open data, https://www.rijdendetreinen.nl/en/open-data/train-archive, 2025, Dataset released under the Creative Commons Attribution 4.0 license.

[25] CARTO, Positron basemap (no labels), https://carto.com, 2024, Basemap tiles by CARTO, under CC BY 3.0. Data by OpenStreetMap, under ODbL. Accessed via the contextily Python package.

[26] D. Ward *et al.*, contextily: Context geo-tiles in Python, https://contextily.readthedocs.io, 2024, Python library for adding web map tiles to geospatial visualizations.

[27] M. D'Alessandro and P. Van Mieghem, Fractional derivative in continuous-time Markov processes and applications to epidemics in networks, Phys. Rev. Res. **7**, 013017 (2025).

[28] C. D. Meyer, *Matrix Analysis and Applied Linear algebra* (SIAM, Philadelphia, PA, 2023).

[29] J. P. Tian and Z. Liu, Coalescent random walks on graphs, J. Comput. Appl. Math. **202**, 144 (2007).

[30] R. Patel, A. Carron, and F. Bullo, The hitting time of multiple random walks, SIAM J. Matrix Anal. Appl. **37**, 933 (2016).

[31] Y. Ji, Q. Wang, X. Li, and J. Liu, A survey on tensor techniques and applications in machine learning, IEEE Access **7**, 162950 (2019).

[32] B. N. Khoromskij, Tensors-structured numerical methods in scientific computing: Survey on recent advances, Chemom. Intell. Lab. Syst. **110**, 1 (2012).

[33] T. G. Kolda and B. W. Bader, Tensor decompositions and applications, SIAM Rev. **51**, 455 (2009).